UNIVERSITY OF GENEVA

MASTER'S THESIS IN CHEMISTRY

Chaperone-like activity of water-soluble gold nanoclusters

Jonnatan Banon

May 2020

Director

Prof. Thomas Bürgi

Supervisor

Dr. Sarita Roy Bhattacharya

I hereafter certify that every statement of this report originating from another source than my personal thoughts has been attributed to its legitimate source, and that every statement directly copied from another source is explicitly mentioned between quotes.

Acknowledgments

First of all, I want to express my thanks to Thomas Bürgi for giving me the opportunity to be part of his research group. It was a big pleasure for me to be part of the group during my master's project.

I would also like to express my grateful to Sarita Bhattacharya, I particularly appreciate the time she dedicated to explaining me all analysis and concepts required to achieve this project. I feel especially lucky to have had her as supervisor of my thesis, her constant motivation, accessibility for discussions and assistance for interpretations of results are highly appreciated.

Further, I would like to thank all Bürgi's lab members for the friendly environment, explanations, and suggestions during the development of my thesis, which would not have been possible in the same quality without their help.

Finally, I would like to thank my family, my fiancée, and friends for the support during all my master.

Résumé

Des conditions neurodégénératives graves et d'autres maladies incurables proviennent de dénaturation des protéines, résultant de l'agrégation d'un groupe diversifié de peptides et des protéines. Les chaperones sont connus pour être efficaces pour supprimer l'agrégation des protéines. Cependant, les chaperones sont difficiles à synthétiser, difficiles à purifier, spécifiques à chaque protéine et coûteux. Par conséquent, il est urgent de trouver des alternatives pour remplacer le rôle des chaperones pendant l'agrégation des protéines. Le but de cette recherche est concentré sur l'étude de l'activité chaperone des nanoclusters d'or solubles dans l'eau ($Au_{25}(SG)_{18}$, $Au_{25}(Capt)_{18}$ et $Au_{68}(3MBA)_{32}$) dans l'agrégation des protéines. Citrate synthétase, aldolase et albumine de sérum bovin en tant que modèles des protéines ont été soumis à une température élevée pour induire l'agrégation *in vitro*.

Les résultats suggèrent que $Au_{68}(3MBA)_{32}$ nanoclusters ont montré une meilleure efficacité pour inhiber l'agrégation des protéines que $Au_{25}(SG)_{18}$ et $Au_{25}(Capt)_{18}$. De plus, l'agrégation des protéines a été réduite lorsque la concentration des Au nanoclusters (NCs) as augmenté. Cette réduction de l'agrégation des protéines en présence d'Au NCs peut être attribuée à la formation initiale du conjugué protéine-NC à l'état de nucléation. Une interaction supplémentaire avec d'autres complexes protéine-NCs provoque une augmentation de la taille des agrégats jusqu'à sa saturation et par conséquent une réduction de l'exposition des domaines hydrophobes des protéines. L'effet protecteur des NCs contre l'agrégation des protéines, même après le début de l'agrégation, prouve que les NCs possèdent une activité "holdase".

Abstract

Serious neurodegenerative conditions and other incurable protein misfolding disease result from the aggregation of a diverse set of peptides and proteins. Chaperones are known to be effective for suppressing protein aggregation. However, chaperones are difficult to synthesize, hard to purify, specific for each protein and costly. Therefore, alternatives to replace the role of chaperones during protein aggregation are urgently needed. The aim of the present research is focused on studying the chaperone-like activity of water soluble gold nanoclusters ($Au_{25}(SG)_{18}$, $Au_{25}(Capt)_{18}$ and $Au_{68}(3MBA)_{32}$) in proteins aggregation. Citrate synthase, aldolase and bovine serum albumin as protein models were subjected to elevated temperature to induce the aggregation *in vitro*.

Results revealed that $Au_{68}(3MBA)_{32}$ nanoclusters showed better efficiency to inhibit aggregation of proteins than $Au_{25}(SG)_{18}$ and $Au_{25}(Capt)_{18}$. Furthermore, aggregation of proteins was reduced when Au nanoclusters (NCs) concentration was increased. This reduction of protein aggregation in presence of Au NCs can be attributed to the formation of initial protein-NCs conjugate in the nucleation state. Further interaction with other protein-NCs complexes cause increasing of aggregates size until its saturation and consequently reducing the hydrophobic exposure areas of proteins. Protective effect of NCs against aggregation of protein even after the initiation of aggregation proves that the NCs possess holdase activity.

Abbreviations

AA	Amino acid
AGE	Advanced glycation end-products
Ag NP	Silver nanoparticle
Ald	Aldolase
ATP	Adenosine triphosphate
Au NC	Gold nanocluster
Au NP	Gold nanoparticle
BSA	Bovine serum albumin
BSA NC	Bovine serum albumin nanocluster
Capt	Captopril
Capt NC	Captopril nanocluster
CS	Citrate synthase
Cys	Cysteine
DHLA	Dihydrolipoic acid
DNA	Deoxyribonucleic acid
FTIR	Fourier-transform infrared spectroscopy
NC	Nanocluster
NP	Nanoparticle
SG	Glutathione
SG NC	Glutathione nanocluster
HSA	Human serum albumin
HSP	Heat-shock protein
IR	Infrared
OD	Optical density
ROS	Reactive oxygen species
SR	Thiolate
TEM	Transmission electron microscopy
UV-vis	Ultraviolet-visible
ZIF	Zeolitic imidazole framework
3MBA	Meta mercaptobenzoic acid
4MBA	Para mercaptobenzoic acid

Contents

1. Introduction

Nanoparticles have been in the focus of attention for many years. However, the structure of these particles is not very well defined, in advantage, metal nanoclusters (*ca.* 1-2 nm) present defined geometry and electronic structure. Metal nanoclusters consist of several to hundreds of metal atoms, bridging the gap between small organometallic complexes and large metal nanoparticles.[1] Metal nanoclusters typically have a core-shell structure, which is composed of a metal core and a protective ligand shell. The unique geometric and electronic structures of metal nanoclusters give rise to many other interesting properties, such as chirality, magnetism, redox chemistry and photovoltaic properties,[2] and permit important technology applications such as catalysis, sensing, medicine, drug or DNA delivery, optics, photonics, and nanotechnology.[3]

1.1. $Au_n(SR)_m$ nanoclusters

Thiol-stabilized atomically precise gold nanoclusters are gaining a lot of importance due to their intriguing properties and applications.[4] The first report on size focused thiolate protected clusters was published by Brust,[5] and in the following years, new synthetic approaches were developed leading to a range of different sizes and structures.[6]

The role of the gold-thiolate surface in the cluster's protection can be summed up to three major contributions: Au-Au interaction, linear S-Au-S bonds and terminal S-Au bonds, as is showed in Figure 1.[6] $Au_n(SR)_m$ nanoclusters (where, SR = thiolate) typically involve organic-soluble ligands, and as a result, the nanoclusters are organic soluble only. On the other hand, water-soluble nanoclusters are highly desirable in many applications.[2]

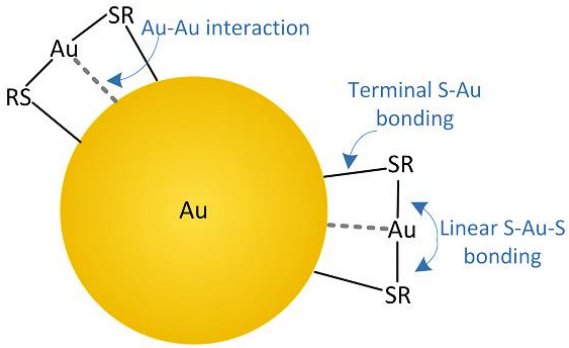

Figure 1. Principal interactions present in gold-thiolate nanoclusters.[6]

Stability of $Au_n(SR)_m$ nanoclusters depend on strength of RS-Au-RS bond and interaction between gold (in staple motifs) and metallic core. The type of staple motif surrounding the gold core makes each cluster structure unique. The four most common synthesized clusters surrounded by monomeric (short) and/or dimeric (long) staples are shown in Figure 2. $Au_{144}(SR)_{60}$ (icosahedral Au_{114} core), $Au_{102}(SR)_{44}$ (Au_{79} core), $Au_{38}(SR)_{24}$ (bi-icosahedral Au_{23} core) and $Au_{38}(SR)_{24}$ (Au_{13} core).[7]

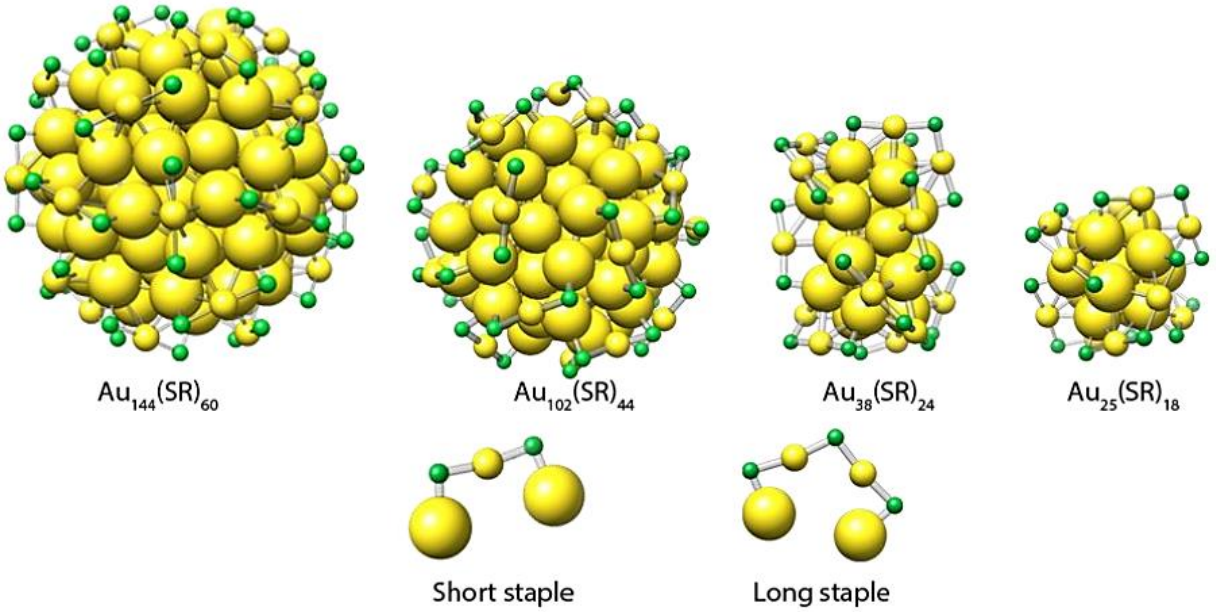

Figure 2. Most common synthesized nanoclusters surrounded by short and/or long staples motifs.[7]

1.2. Water soluble gold nanoclusters

Some water-soluble gold nanoclusters have been synthesized for their highly desirable applications in life science and medicine, high biocompatibility, good photo-stability, low toxicity, and their use in cell labeling, phototherapy, and biosensing.[8]

The water-soluble nature of nanoclusters depends on the solubility of thiol ligands. Glutathione (SG),[4] captopril (Capt),[2] meta-mercaptobenzoic acid (3MBA),[9] cysteine (Cys),[10, 11] and para-mercaptobenzoic acid (4MBA)[12] are most studied ligands for the synthesis of water-soluble gold nanoclusters in recent years. Others thiol ligands like 4-mercaptobutyric acid, 3-mercapto-1,2-propanediol, thiomalate, tiopronin, methionine, 2-mercaptobenzoic acid, selenomethionine, 1-thio-*β*-D-glucose and a pentapeptide (sequence Ile-Thr-Cys-Ala-Glu) were also used to synthesize water soluble monolayer-protected gold clusters.[13]

Water soluble nanocluster applied principally as fluorescent probes for sensing and imaging were also synthesized. For example glucose-conjugated Au NCs have been used as a target-specific fluorescent probe to detect glucose metabolism in cancer cells.[14] Cyclodextrin-capped Au NCs have been used as a label-free fluorescent nanosensor for specific detection of heavy metal in mammalian cells.[15] Oligoarginine-capped Au NCs showed capability for intracellular imaging of reactive oxygen species (ROS) in living cells and zebrafish.[16] *β*-Lactoglobulin stabilized Au NCs served as intracellular imaging and sensor for detecting Hg^{2+} in beverage, urine, and serum with high sensitivity,[17] and bovine serum albumin-capped gold nanoclusters had excellent selectivity to sense Hg^{2+} in different aqueous samples.[18]

Recent advancements have been applied in water soluble Au NCs with different surface modification as antimicrobial agents, as an example mannose-capped Au NCs were found to be efficient antibacterial agents against *E. coli* by inducing agglutination.[19] Mercaptohexanoic acid protected Au NCs presented interaction with Gram-positive and Gram-negative bacteria, increasing intracellular ROS production and consequently antimicrobial effect.[20] Quaternary ammonium-capped Au NCs have shown to be antimicrobial agents against Gram-positive bacteria like *S. aureus* and *Enterococcus spp.* through catalytic generation of ROS and disturbance of intracellular metabolic pathway.[21]

In the present study $Au_{25}(SG)_{18}$, $Au_{25}(Capt)_{18}$ and $Au_{68}(3MBA)_{32}$ were chosen as water gold soluble nanoclusters because of their ease of synthesis method, good thermal stability, and promising biocompatibility.

1.2.1. $Au_{25}(SG)_{18}$

Glutathione (SG) capped Au NCs are widely studied because of their easily accessible synthetic availability, great biocompatibility, and facile further surface functionalization for biological application.[22] This nanocluster is highly biocompatible due to the presence of glutathione ligand and exhibits good photo thermal activity which permits its use for in vitro photothermal therapy of breast cancer cells,[4] glutathione contains some electron-rich groups (e.g. carboxylic and amino groups), and these groups can possibly interact with the gold cluster surface and directly donate the delocalized electron density to the gold core (Figure 3), electron-rich atoms like O and N in glutathione should result in larger enhancement of fluorescence.[23]

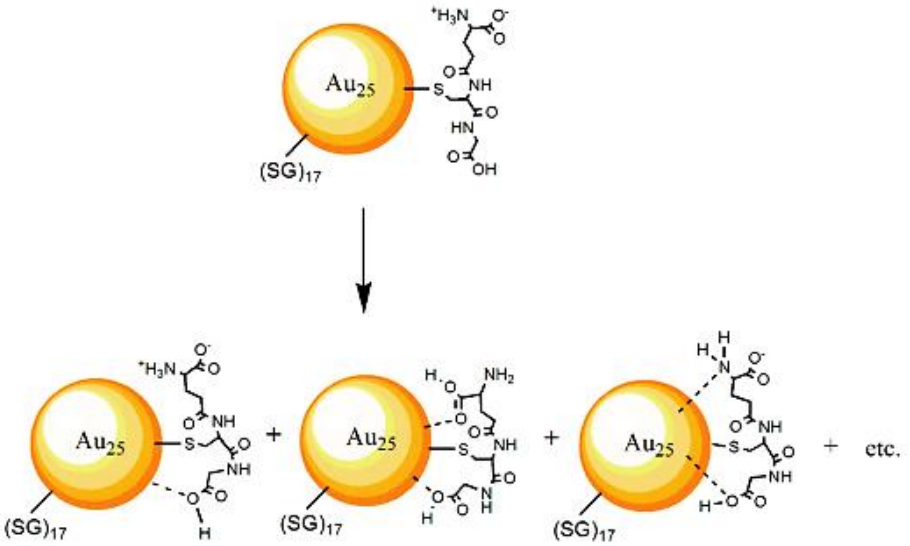

Figure 3. Possible interaction of amine and carboxyl groups of glutathione ligands to the gold surface.[23] Reprinted with permission from Wu, Z. et al. *Nano Letters* 2010, 10 (7), 2568-2573. Copyright (2010) American Chemical Society.

The UV-visible absorption spectra of $Au_{25}(SG)_{18}$ showed absorption bands at 400, 450 and 670 nm, and TEM image of the nanoclusters shows a uniform size of ~1 nm (Figure 4).[4]

Many applications using $Au_{25}(SG)_{18}$ were developed. A general strategy was performed to uniformly encapsulate $Au_{25}(SG)_{18}$ into ZIF-8 (Zeolitic imidazolate framework) by coordination-assisted self-assembly.[24] Another interesting application of $Au_{25}(SG)_{18}$ was achieved using human serum albumin (HSA) to induce the aggregation-enhanced emission of GS-Au NCs through hydrophobic and electrostatic interaction between them.[25]

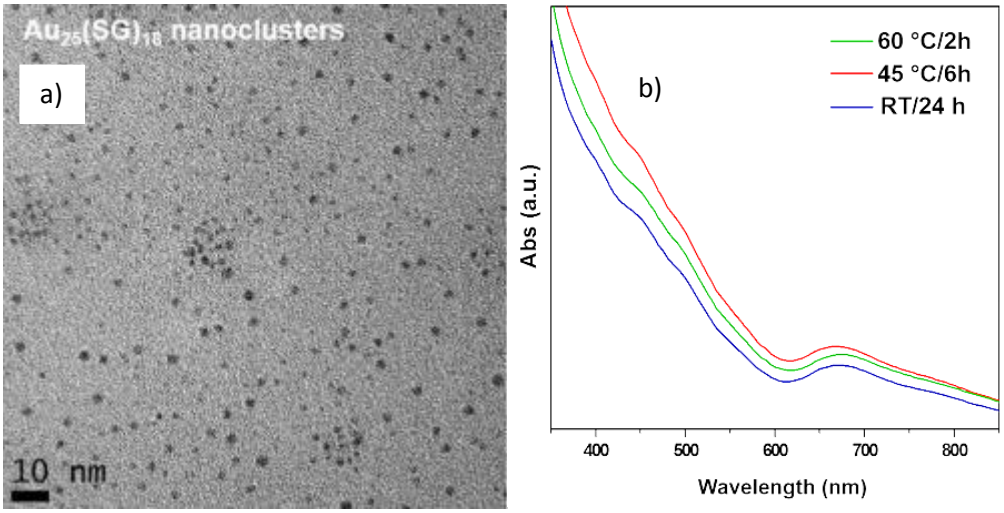

Figure 4. a) TEM image and **b)** UV-vis absorption spectrum of $Au_{25}(SG)_{18}$ formed at different temperatures (room temperature, 45 and 60 °C).[4] Adapted with permission from Katla S. K. et al. *ACS Applied Materials & Interfaces* **2018,** *10* (1), 75-82. Copyright (2018) American Chemical Society.

1.2.2. $Au_{25}(Capt)_{18}$

Captopril is highly favored water soluble ligand for the synthesis of nanocluster. Because of the presence of five-membered pyrrolidone ring, it provides structural rigidity and better stability than other ligands like glutathione. $Au_{25}(Capt)_{18}$ possess a much higher thermal stability than other water soluble nanocluster in solution.[2] The CD spectra of $Au_{25}(Capt)_{18}$ shows two strong positive bands (at 275 and 480 nm) and two negative bands (at 310 and 430 nm). The vibrational circular dichroism (VCD) spectrum of $Au_{25}(Capt)_{18}$ has a characteristic bi-polar peak (positive-negative from high to low wavenumbers) ranging from 1620 – 1560 cm^{-1}.[26] $Au_{25}(Capt)_{18}$ nanoclusters are stable in the pH range from 4 to 10 in water,[27] and its UV-visible absorbance spectrum shows two principal characteristic peaks at 670 and 450 nm with some shoulder peaks around 550 and 400 nm (Figure 5).[26]

The water solubility, high thermal stability, and chirality of the $Au_{25}(Capt)_{18}$ nanocluster make this material quite promising for further biological applications.[2] A new hydrogel nanoparticle was made by synthesizing polyacrylamide-encapsulated $Au_{25}(Capt)_{18}$ nanoparticles to improve its conjugation with targeting agents and to enhance biocompatibility.[28] On the other hand, generation of highly reactive singlet oxygen ($^1O_2$) (important for a variety of applications such as photodynamic therapy for cancer treatment, water treatment, catalytic oxidation, and others) was efficiently produced through the direct photosensitization by $Au_{25}(Capt)_{18}^-$ clusters.[29]

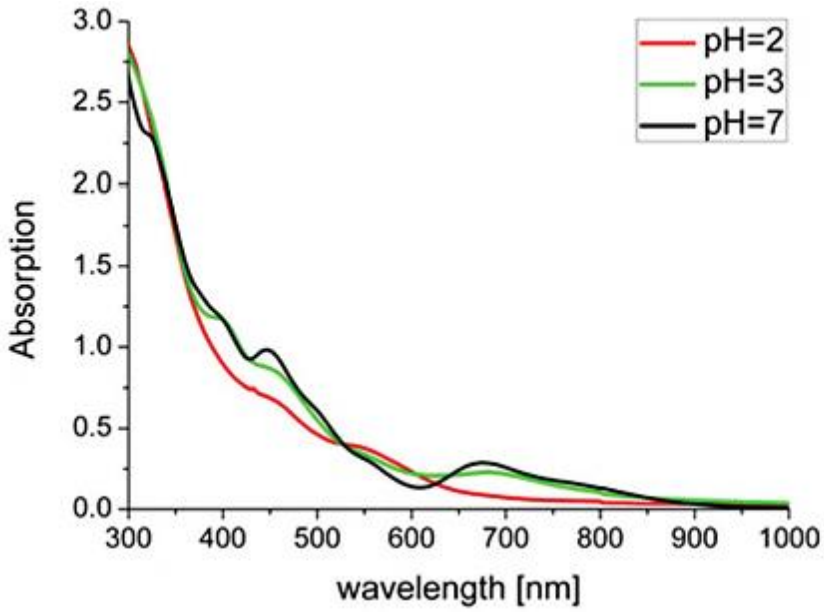

Figure 5. UV-visible absorbance spectrum of $Au_{25}(Capt)_{18}$ dispersed in water at different pH.[27] Reprinted with permission from Waszkielewicz, M. et al. *Nanoscale* 2018, 10 (24), 11335-11341. Copyright (2018) The Royal Society of Chemistry.

1.2.3. $Au_{68}(3MBA)_{32}$

Water-soluble gold nanoparticles have also been formed with 3MBA. The 3MBA-proteceted nanoclusters is of particular interest for its high reactivity toward other thiol compounds including protein sulfhydryl groups and its exceptional utility in bioconjugation.[9]

$Au_{68}(3MBA)_{32}$ has a structure based almost entirely on local fcc packing and deviates from spherical shape.[30] The synthesized $Au_{68}(3MBA)_{32}$ is homogeneous in size, stable in solution, and reactive toward sulfhydryl compounds, including proteins. The UV-visible absorbance spectrum is featureless.[30] The IR spectrum of $Au_{68}(3MBA)_{32}$ showed four peaks in the range 2500 – 3700 cm^{-1} consistent with OH-stretching vibrations of water at various degrees of hydrogen-bonding, and also four characteristic peaks below 1800 cm^{-1} confirming ligand vibration, another discrete absorption peak at ~4200 and 5250 cm^{-1} and a split transition at 6100 cm^{-1} (Figure 6).[30]

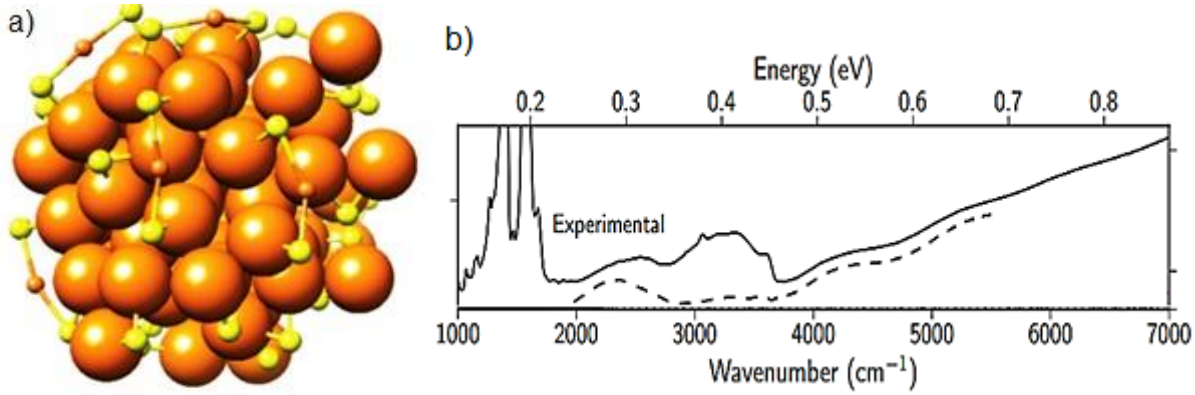

Figure 6. a) model structure **b)** and IR spectrum of $Au_{68}(3MBA)_{32}$ nanocluster.[30] Adapted with permission from Azubel, M. et al. *Science* 2014, 345 (6199), 909-912.Copyright (2014) American Association for the Advancement of Science.

1.3. Au nanoclusters and proteins bioconjugation

The development of Au water-soluble nanoclusters in recent years opened the possibility of NCs to be used in bio-applications. Many studies were made on bio-conjugation with Au NCs by surface modification via antibodies, peptides, polymers, and small bio-organic molecules: sugars like glucose[14] and mannose[19], peptides like oligoarginine[16] and proteins like β-lactoglobulin[17] were used to form capped Au NCs for specific biological applications. Also many proteins have been used as stabilizing agents for Au NCs such as BSA,[31] lysozymes,[32] human transferrin,[33] lactoferrin,[34] trypsin,[35] pepsin,[36] insulin,[37] and horseradish peroxidase.[38]

Further works to study interaction with proteins were made. A study of interaction between Au nanocluster (GS-Au NCs) and human serum albumin (HSA) was performed to induce aggregation and significantly enhance luminescence emission of nanoclusters (aggregation-enhanced emission).[25] Furthermore, dihydrolipoic acid (DHLA) protected gold nanoclusters (DHLA-Au NCs) were used to study its interaction with HSA and transferrin as model proteins. Results showed that DHLA-Au NCs could induce agglomeration of proteins which requires further study in the future.[39] However, there is no previous reported study about the role of Au nanoclusters in protein aggregation. Elucidating the potential chaperone activity of soluble Au NCs in proteins could provide new approaches in this field.

1.4. Proteins

Proteins are the most versatile and abundant organic compound in animals. They are composed of C, H, O, N, and S, and are polymers with more than 6000 kDa. The proteomes of mammalian cells typically comprise between 10 000 and 20 000 different proteins. The abundance of each protein, required for its biological activity, is encoded in the linear amino acids (AA) sequence of the newly synthesized polypeptide chain, which may be up to several thousand AAs in length.[40] Twenty AAs are obtained after complete hydrolysis of proteins.[41]

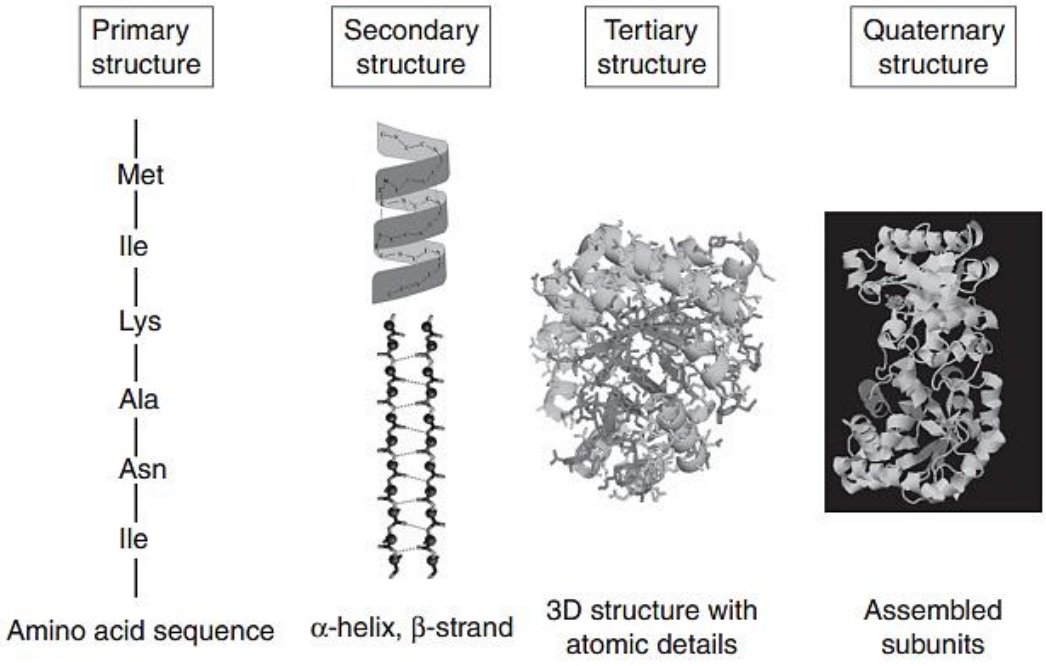

Figure 7. Different levels of protein structure.[42] Reprinted with permission from Gromiha M., *Protein Bioinformatics*, 2010; pp 1-27. Copyright (2010) Elsevier.

Protein structure is described in four levels, primary structure of proteins consists of the basic amino acid sequence, the correct three-dimensional conformation of protein requires protein folding. This transforms the linear AA sequence into more complex spatial arrangements with alpha-helices and beta-pleated sheets called the secondary structures. Further folding gives rise to a three-dimensional globular protein with a particular tertiary structure. Association with other proteins may occur, to form a multi-protein complex with its own quaternary structure (Figure 7).[43]

Two general types of proteins can be distinguished: Globular proteins, which fold and form a compact spheroid or ovoid with three axes of similar length, they disperse well in aqueous media and in general, they are functionally active proteins, such as enzymes, antibodies, hormones and hemoglobin. Fibrous proteins consist of parallel peptides chains that form extended fiber or sheets, with the longitudinal axis markedly predominating over the transversal one. In general, these proteins do not disperse in water, and form a part of structures that require great physical strength, such as the connective tissue fiber.[41]

In the present work, citrate synthase, aldolase and bovine serum albumin were chosen as model proteins to study its aggregation in presence of Au NCs. These proteins were chosen because they are involved in crucial living mechanism, CS plays a key role in Kreb's cycle, important in cell respiration and production of NADH and FADH2 for electron transport chain. Aldolase is involved in cell glycolysis, to break down glucose into energy, and BSA presents 76% sequence identity with HSA, which is the most abundant carrier in the circulatory system and play major role in transportation and disposition of many endogenous and exogeneous compounds. All these proteins are commercially available.

Citrate Synthase (CS) is a central enzyme in the process of sugar oxidation, first step of the citric acid cycle also known as the Krebs cycle, this enzyme is responsible for the condensation of acetyl-CoA and oxaloacetate to form citrate. The overall structure of citrate synthase is a homodimer composed of two identical monomeric subunits of 437 AAs residues each. The combined weight of the two subunits in the homodimer is 85 kDa.[44] At 43 °C, CS is readily inactivated and subsequently aggregates. Thermal folding analysis of CS aggregation has revealed the presence of two dimeric unfolding intermediates, which are in equilibrium with the native state, before forming the irreversible aggregates.[45]

Aldolase (Ald) plays an important role in glucose metabolism. It has a molecular weight of 160 kDa. Three aldolase isoenzymes have been identified (A, B and C). The aldolase isozymes (A, B, and C) are the same in their overall fold and active site structure.[46] The enzyme is present probably in all cells and occurs in particularly large quantities in muscles, liver, brain. It is localized in both, the cytoplasm and nucleus.[47] A molecule of aldolase is a tetrameric protein with 4 exposed thiol groups (Cys-71, Cys-239, Cys-289 and Cys-338) [48].

Bovine Serum Albumin (BSA) is the most abundant plasma protein in bovines, and it has a single polypeptide chain consisting of about 583 amino acid residues and no carbohydrates. The protein has a molecular weight of 69 kDa. It contains no phosphorus, 17 disulfides and one free sulfhydryl group. In blood plasma albumin is a carrier of free fatty acids.[49] Aggregation of BSA starts with unfolding the native form, which results in formation of two forms of the unfolded protein with different propensity to aggregation. One of the forms (highly reactive unfolded forms) forms primary aggregates. The second form (low reactive unfolded form) can self-aggregate and form small size aggregates or can join to primary aggregates and form secondary aggregates of bigger sizes. Further aggregation of BSA is a result of sticking of secondary aggregates.[50]

Figure 8. Crystal structure of **a)** citrate synthase (PDB: 5CSC),[51] **b)** aldolase (PDB: 1ADO)[52] and **c)** BSA proteins (PDB: 1J4E).[53]

1.5. Folding protein

Proteins must fold to their active native state when they emerge from the ribosome and when they repeatedly unfold and refold during their lifetime (Figure 9).[43] It was inferred that proteins must fold to their unique native state through multiple unpredictable routes and intermediate conformations (Figure 10).[54] The majority of protein molecules must fold into

definite three-dimensional structures to acquire functional activity. However, protein chains can adopt a multitude of conformational states, and their biologically active conformation is often only marginally stable.[40] Native states of proteins almost always correspond to the structure that are most thermodynamically stable under physiological conditions. Natural selection has enabled proteins to evolve so that they are able to fold rapidly and efficiently.[55] A denatured protein is typically 5 - 10 kcal/mol less stable than its native state; therefore, there is no single force contribution solely to destabilization, and there are numerous possible conformations between and within the denatured and native states.[56]

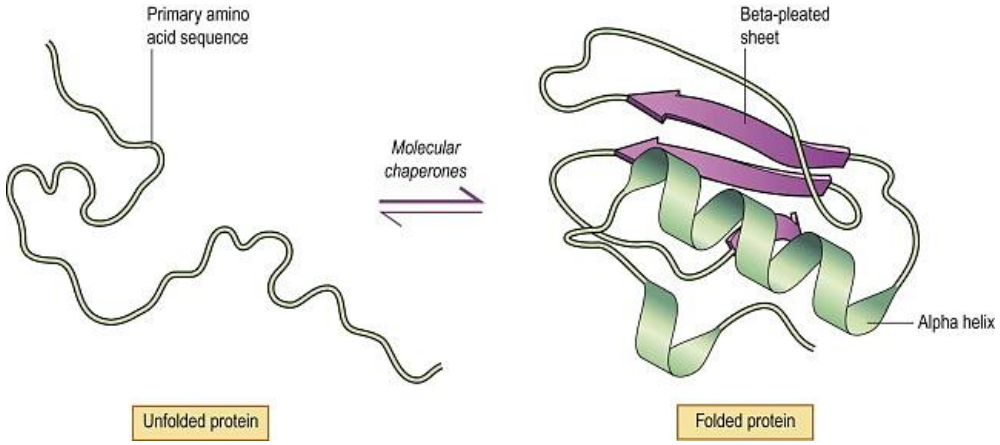

Figure 9. Unfolded and folded protein through interaction with molecular chaperones.[43] Reprinted with permission from Johns, P., *Clinical Neuroscience*, 2014; 91-103. Copyright (2014) Elsevier.

Conformational stability of a protein molecule depends not only on the amino acid sequence of the polypeptide chain, the role of solvent is also of important for its stability. In water, protein structure represents a delicate balance between conformational entropy, which tend to unfold the protein, and various stabilizing energy contributions such as hydrogen bonds, hydrophobic and Van der Waals interactions, and electrostatic forces.[57] Large numbers of misfolded proteins may aggregate in the cytoplasm.[43] In the case of soluble proteins, hydrophobic forces are particularly important in driving chain collapse and putting non-polar AAs residues within interior of protein during folding.[58] Free energy of protein stabilization is small compared with destabilizing contributions, therefore fluctuations of the environments (temperature, pH, ionic strength, or ligand binding) might destabilize or contrary, might provide extra stabilization of the protein.[57]

1.6. Protein aggregation

Protein aggregation denotes the process by which protein molecules assemble into stable complexes composed of two or more proteins, with the individual proteins denoted as the

monomer. Aggregates are often held together by strong non-covalent contacts, and require some degree of conformational distortion (unfolding or misfolding) in order to expose key AAs that form the strong contacts between monomers.[59]

Protein aggregation can be reversible or irreversible and the aggregates formed can be soluble/insoluble, covalent/non-covalent and native/non-native. The large number of different theories and models that have been proposed to describe protein aggregations demonstrate that the phenomenon varies significantly depending on the aggregation conditions and the protein studied (Figure 10).[60]

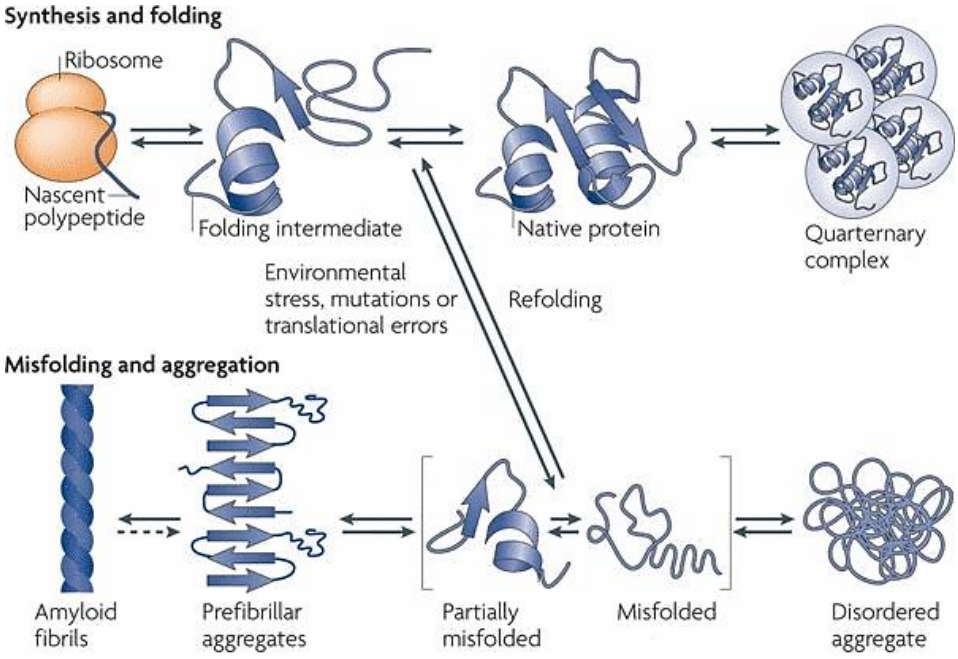

Figure 10. Different pathways to protein aggregation and conformational choices.[61] Adapted with permission from Tyedmers, J. et al. *Nature Reviews Molecular Cell Biology* 2010, 11 (11), 777-788.. Copyright (2010) Springer Nature.

Metastable proteins tend to populate misfolded species that are prone to forming toxic aggregates, including soluble oligomers and fibrillar amyloid deposits, which are linked with neurodegeneration disease, and many other pathologies. To prevent or regulate protein aggregation, all cells contain an extensive protein homeostasis or proteostasis network comprising molecular chaperones and other factors. These defense systems tend to decline during aging, facilitating manifestation of aggregates deposition disease.[40]

1.7. Molecular chaperones

Molecular chaperones are any protein that interacts with, stabilizes or helps another protein to acquire its functionally active conformation, without being present in its final

structure.[58] Molecular chaperones are diverse and also play other roles apart of assisting folding and assembling nascent protein chains. They can refold proteins, assist proteins trans-location through membranes, and facilitate proteins degradation.[62] In stressed cells, many sensitive proteins may alternate between native and partially unfolded states, which, depending on the conditions and the presence of seeds, may choose to aggregate or revert to the native state. Molecular chaperones can control such interactions by sequestering active seeds and aggregation-prone intermediates.[63]

Although small proteins may fold at very fast speeds (within microseconds), in dilute buffer solutions, larger, multidomain proteins may take minutes to hours to fold. And often even fail to reach their state in vivo. Requirement for molecular chaperones respond to the need to minimize protein aggregation during folding and maintain proteins in soluble state.[58]

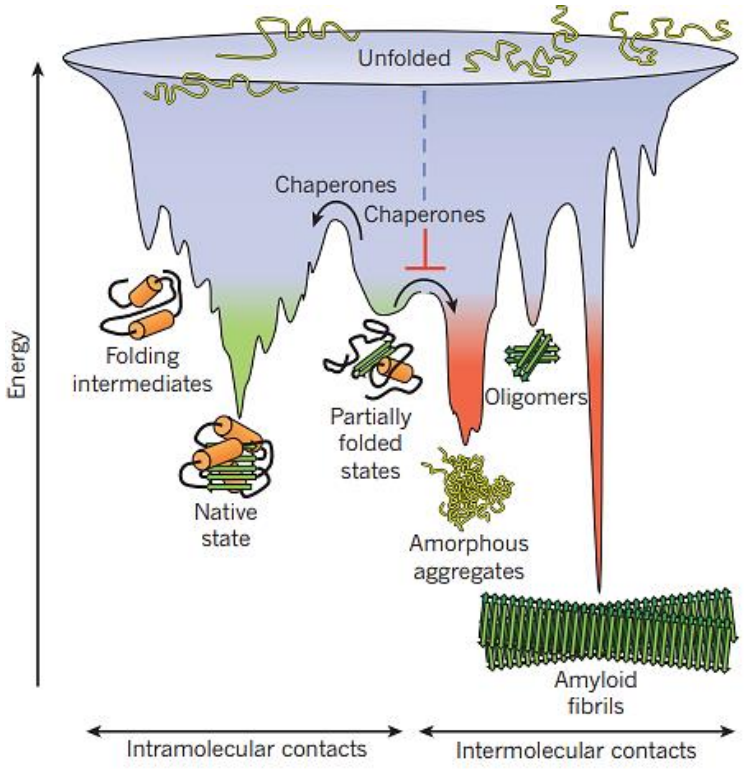

Figure 11. Scheme of the funnel-shaped free-energy surface that proteins explore as they move towards the native state by forming intramolecular contacts.[58] Reprinted with permission from Hartl, F. U. et al. *Nature* 2011, 475 (7356), 324-332.Copyright (2011) Springer Nature.

In the current model, polypeptides chains are thought to explore funnel-shaped potential energy surfaces as they progress, along several downhill routes, towards the native structure (Figure 11). Proteins move towards the native state through different steps and by forming intramolecular contacts. In vivo, these steps may be accelerated by

chaperones. In this model, partially folded or misfolded states are problematic because they tend to aggregate in a concentration-dependent manner. These forms typically expose hydrophobic amino-acid residues and regions of unstructured polypeptide backbone to the solvent – features that become buried in the native state. Thus, aggregation is largely driven by hydrophobic forces and primarily results in amorphous structures.

Several different classes of structurally unrelated chaperones exist in cells, forming cooperative pathways and networks. Members of these protein families are often known as stress proteins or heat-shock proteins (HSPs), chaperones are usually classified according to their molecular weight (HSP40, HSP60, HSP70, HSP90, HSP100 and the small HSPs).[58] Molecular chaperones have been divided also into three functional subclasses based on their mechanism of action. Folding chaperones, which rely on ATP-driven conformational changes to mediate the net refolding/unfolding of their substrate. Holding chaperones, which maintain partially folded proteins on their surface to await availability of folding chaperones upon stress abatement. The third class of chaperones promotes the solubilization of proteins that have become aggregated as a result of stress.[64]

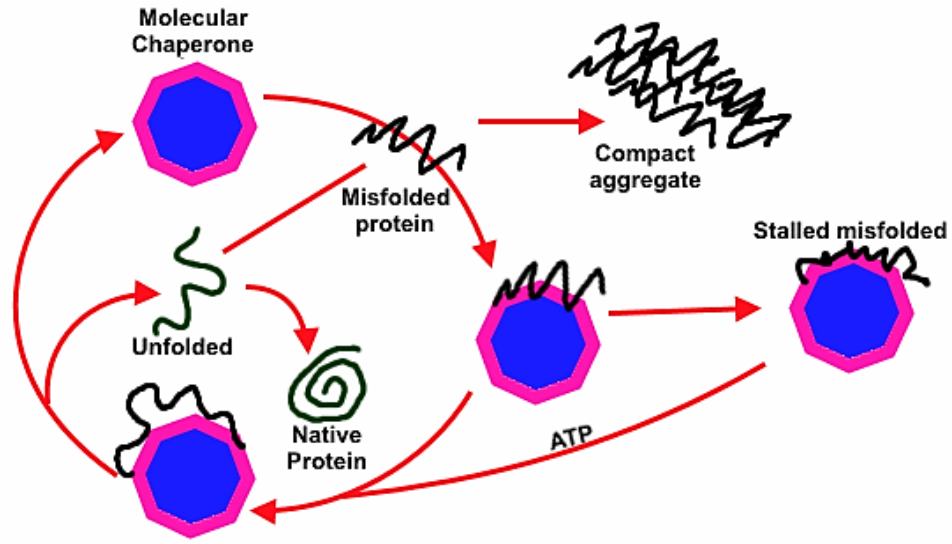

Figure 12. General mechanism for holding molecular chaperones.

In holding molecular chaperones, a general mechanism is known: A misfolded polypeptide chain may be assembled into a compact aggregate relatively resistant to chaperons or bind to specific hydrophobic surface on a molecular chaperone. When binding does not sufficiently unfold the misfolded species, catalytic sites of the chaperone become stalled

by over-sticky misfolded species. When binding productively unfolds the misfolded species, this forms a partially unfolded species that may start refolding and consequently dissociate from the chaperone surface, and either spontaneously refold to the native state or misfold again and re-enter the chaperone cycle. The energy of ATP hydrolysis may be used to forcefully unfold severely misfolded and aggregated species which, after chaperone release can spontaneously reach the native state (Figure 12).[65]

1.8. Protein stabilization with Au NCs

Protein stabilization is a natural process in which biological organism intake metal species to subsequently form mineral structures. Bio-organism or macromolecules have a natural ability to intake and arrange inorganic molecules. Based on this phenomenon, proteins with gold atom precursors can evolve producing stable and fluorescent Au NCs (Figure 13). There are many advantages of this approach, relatively low environmental impact, mild reaction conditions, aqueous solutions chemistry and absence of strong reducing agents. Only pH condition in the reaction is altered to optimize protein's reducing ability.[66]

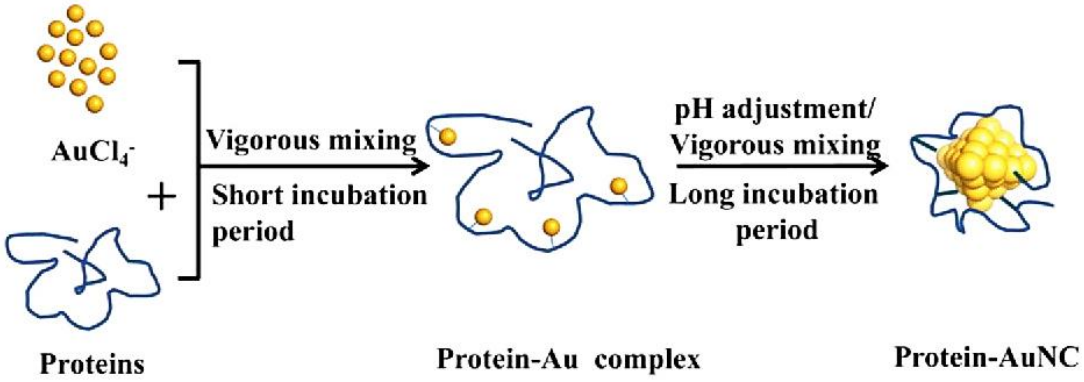

Figure 13. Pathway for producing Au NCs with selected proteins that promote NC growth and formation.[67] Reprinted with permission from Li, C. et al. *Critical Reviews in Food Science and Nutrition* 2018, 58 (5), 689-699. Copyright (2018) Taylor & Francis.

Amino acids are randomly organized in peptide strands and only certain sequences of amino acids can promote nanoparticles growth while others will have little interaction with metal ions.[68] Formation of a single Au NCs following this technique is highly dependent on the conformation of the protein. It is already know that selected AAs can play a key role in nanoclusters synthesis due to their reducing strength and/or favorable binding interaction with gold atoms. [66]

1.9. Motivation

Serious neurodegenerative conditions, including Alzheimer's disease, Parkinson's disease, Huntington's disease and prion disease, result from the aggregation of a diverse set of peptides and proteins.[69] In some cardiovascular diseases, cataract, alcoholic hepatitis, cystic fibrosis. phenylketonuria, and in a range of human cancers the protein homeostasis machinery was also shown to be involved as the first line of defense against the disease. Aggregated proteins result from failure or stress during this mechanism, thus becoming it a molecular marker for diagnostics.[62]

Misfolding has been linked to a rapidly expanding list of pathologies. Two groups of these diseases must be distinguished: loss-of-function and toxic gain-of-function diseases. Pathologies include cystic fibrosis, neurodegenerative diseases, as well as type II diabetes and certain forms of heart disease and cancer. The majority of cases are manifested in an age-dependent manner, apparently facilitated through a decline in the capacity of the proteostasis network that occurs during aging.[40]

Chaperones are known to be effective for suppressing protein aggregation in micromolar concentration. However, chaperones are difficult to synthesize, hard to purify, specific for each protein and costly.[70] Therefore, alternatives to replace the role of chaperones during protein aggregation is urgently needed. Some researches were made to study the chaperone activity of gold nanoparticles in proteins as an alternative. Anti-glycation activity of gold nanoparticles (Au NPs) in chaperone α-crystallin was performed to prevent the formation of advanced glycosylic end products (AGEs), which is known to affect activity of chaperones, leading formation of aggregates.[71] AGEs formation was significantly minimized with Au NPs and Ag NPs synthesized enzymatically by β-galactosidase enzyme.[72] Interaction of citrate-capped Au NPs/Ag NPs with HSP18 chaperone was developed showing that chaperone function of HSP18 is enhanced upon Au NPs interaction and reduced upon interaction with Ag NPs.[73] For the formation of HSA related AGEs in presence of Au NPs, it was found that concentration of HSA and glyceraldehyde mixture resulted in lower reaction rate after being incubated with Au NPs.[74] Chaperone activity of human HSPB1 (B1 N-terminal region) conjugated gold nanoparticle was demonstrated to have therapeutic potential to prevent protein aggregation.[75] Au NPs prevent significantly (up to 95 %) thermal and chemical aggregation of two unrelated proteins of different size, alcohol dehydrogenase (84 kDa) and insulin (6 kDa) in

physiological pH.[70] Finally, gold nanoparticles (20 and 40 nm) have shown to prevent the thermal aggregation of citrate synthase.[76]

Despite the different studies related to the chaperone like activity of Au NPs and its effect through interaction with proteins, there is no published research on Au NCs and its potential effect as chaperone agent to prevent protein aggregation, opening a potential field of study for water soluble nanoclusters.

1.10. The aim of the project

The aim of the present research is focused on studying the chaperone-like activity of water soluble gold nanoclusters ($Au_{25}(SG)_{18}$, $Au_{25}(Capt)_{18}$ and $Au_{68}(3MBA)_{32}$). CS, aldolase and BSA as protein models were subjected to elevated temperature to induce the aggregation of proteins *in vitro* and later the protective nature of Au NCs has been studied. Formation of protein-NCs conjugate and prevention of protein aggregation have been characterized by a variety of scattering and spectroscopic techniques.

2. Materials and Methods

2.1. Chemicals

All the chemicals were commercially available and used without further purification. Hydrogen tetrachloroaurate(III) trihydrate ($HAuCl_4 \cdot 3H_2O$, Alfa Aesar, 99.99%), tetraoctylammonium bromide (TOABr, Alfa Aesar, >98%), captopril ($C_9H_{15}NO_3S$, Sigma Aldrich, ≥98%), L-glutathione reduced ($C_{10}H_{17}N_3O_6S$, Carl Roth, ≥99%), meta-mercaptobenzoic acid (3MBA, Fluorochem, >97.0%), sodium borohydride ($NaBH_4$, Sigma Aldrich, 99%), sodium hydroxide (NaOH, Acros Organics, 98.5%), methanol and ethanol (Fisher chemical, analytical reagent grade), sodium chloride (Sigma Aldrich, >99.5%, for analysis), bovine serum albumin (lyophilized powder, ≥98%), aldolase type IV from rabbit muscle (Sigma Aldrich, 22 mg protein/ml, in ammonium sulfate suspension), citrate synthase from porcine heart (Sigma Aldrich, 8.8 mg protein/ml, in ammonium sulfate suspension). A 1.0 mg/mL stock solution of citrate synthase and aldolase and a 10 mg/mL stock solution of BSA were prepared in autoclaved Milli-Q water. Water was purified with a Milli-Q system (≥18 MΩ cm).

2.2. Synthesis of $Au_{25}(SG)_{18}$ nanoclusters

The synthesis of $Au_{25}(SG)_{18}$ was done at room temperature under air, following a previous reported method.[4] 0.013 mmol $HAuCl_4 \cdot 3H_2O$ (5 mg) was first dissolved in 10 mL of Milli-Q water. 0.052 mmol L-glutathione reduced (16 mg) dissolved in 10 mL of Milli-Q water was added to the previous solution under stirring. The solution changed from yellow-orange to cloudy white color, indicating the reduction of Au(III) to Au(I). 0.132 mmol $NaBH_4$ (5 mg) freshly dissolved in 10 mL of Milli-Q water was added to the previous prepared mixture. The reduction of Au(I) to Au(0) happened and the solution instantaneously changed to brown color and effervescence happened because of the reduction of borohydride. The reaction continues with the solution vial placed into a water bath at 60 °C for 2 h to complete the formation of $Au_{25}(SG)_{18}$ nanoclusters. Concentration of the solution to 2 mL was then performed using rotavapor at 40 °C under low pressure. 10 mL of methanol was added to the previous solution and centrifugated at 8 000 rpm for 20 min at 14 °C to precipitate the nanoclusters. After decantation of the supernatant, the dark brown precipitate was dispersed in Milli-Q water and the methanol washing was repeated. The concentrated precipitate thus obtained was redispersed in Milli-Q water and dried using lyophilization for further characterization.

2.3. Synthesis of $Au_{25}(Capt)_{18}$ nanoclusters

$Au_{25}(Capt)_{18}$ was prepared as was described early[26] using methanol as solvent, at room temperature under air. 20 mmol $HAuCl_4 \cdot 3H_2O$ (78.7 mg) and 0.23 mmol TOABr (126.8 mg) were dissolved and mixed in 10 mL methanol under vigorous stirring to promote the ligand exchange between $HAuCl_4$ and TOABr and the color changed from yellow-orange to deep red. After approximately 25 min, 1 mmol captopril (217.2 mg) dissolved in 5 mL of methanol was rapidly added to previous mixture under constant stirring. The reduction of Au(III) to Au(I) happened and the solution color quickly changed to white. After 30 min, 2 mmol $NaBH_4$ (75.6 mg) was dissolved in 5 mL ice cold water and rapidly added to the reaction mixture under vigorous stirring. The mixture color changed to brown-black indicating the reduction of Au(I) to Au(0). The reaction continues under stirring for at least 8 h, the reaction mixture turned to reddish brown color and was centrifugated (8000 rpm, 20 min, 14 °C) to precipitate and remove unreacted, insoluble Au-thiolates polymers. The supernatant was collected and concentrated by rotary evaporation at 35 °C under low pressure. Ethanol was added to the concentrated solution to precipitate the nanoclusters. The precipitated nanoclusters were separated using decantation and centrifugation (8000 rpm, 20 min, 14 °C), and washed with minimum amounts of methanol at least two times.

The nanoclusters were dried in rotavapor (35 °C, under vacuum), re-dispersed in Milli-Q water and finally dried using lyophilization to obtain a dry powder of $Au_{25}(Capt)_{18}$ nanoclusters.

2.4. Synthesis of $Au_{68}(3MBA)_{32}$ nanoclusters

The synthesis of $Au_{68}(3MBA)_{32}$ was based on a method reported previously.[9] 84 mM 3-MBA (8.6 mg) and 28 mM $HAuCl_4 \cdot 3H_2O$ (11 mg) were freshly dissolved in methanol and mixed in a 2:1 molar ratio. Milli-Q water (2.5 volumes) was added, and the pH was adjusted to 13 with NaOH (~26 mg) to dissolve insoluble white precipitate. The mixture was equilibrated for at least 16 h on a rocking platform at room temperature until the solution changed from yellow to colorless. To the previous solution, Milli-Q water and methanol were added to obtain a solution of 2.72 mM 3-MBA, 1.36 mM $HAuCl_4$ and 27 % (v/v) methanol. A freshly prepared solution of 150 mM $NaBH_4$ in Milli-Q water was added to a final concentration of 2 mM $NaBH_4$. After mixing for 4.5 h on a rocking platform at room temperature the reaction was stopped and the nanoclusters precipitated with 100 mM NaCl and 2 volumes of methanol, and separated by immediately centrifugation (10 min, 5000 rpm). The nanoclusters were washed with 75 % methanol, dried in air overnight, resuspended in Milli-Q water and dried again using lyophilization to obtain a dry powder.

2.5. Thermal aggregation of CS at 45 °C

Aggregation of citrate synthase (32 µg/mL) in 10 mM Tris-HCl buffer at pH 7.2 was followed by measuring the turbidity (OD at 360 nm) for 60 min at 45 °C on a Varian Cary 50 spectrophotometer whose temperature is controlled with a Braun Thermomix 1460 heater, using a quartz cuvette of 10 mm path length, first with CS only as a control, and after in presence of $Au_{25}(SG)_{18}$ (30, 50, 80 and 120 µg/mL), $Au_{25}(Capt)_{18}$ (30, 50, 80 and 120 µg/mL) and $Au_{68}(3MBA)_{32}$ (1.7, 6.7 and 12.5 µg/mL). Tris-HCl buffer solution was pre-heated for 8 min until reaching 45°C in absence of CS before the assay.

2.6. Thermal aggregation of aldolase at 60 °C

Aggregation of aldolase (150 µg/mL) in 50 mM phosphate buffer at pH 7.2 was performed by measuring OD at 360 nm for 15 min at 60 °C on a Varian Cary 50 spectrophotometer whose temperature is controlled with a Thermomix 1460 recirculating heater, using a quartz cuvette of 10 mm path length, first with aldolase only as a control, and after in presence of $Au_{25}(SG)_{18}$ (125, 250 and 375 µg/mL), $Au_{25}(Capt)_{18}$ (50, 125 and 250 µg/mL)

and $Au_{68}(3MBA)_{32}$ (16.7, 25.0 and 33.4 µg/mL). Phosphate buffer solution was pre-heated for 8 min until reaching 60 °C in absence of aldolase before the assay.

2.7. Thermal aggregation of BSA at 70 °C

Aggregation of BSA (1 mg/mL) in 10 mM Tris-HCl buffer at pH 7.2 was studied by measuring OD at 360 nm for 40 min at 70 °C on a Varian Cary 50 spectrophotometer whose temperature is controlled with a Thermomix 1460 recirculating heater, using a quartz cuvette of 10 mm path length, first with BSA only as a control, and after in presence of $Au_{25}(SG)_{18}$ (30, 50, 80 and 120 µg/mL). Tris-HCl buffer solution was pre-heated for 8 min until reaching 70°C in absence of BSA before the assay.

2.8. Thermal aggregation of CS after adding Au NCs at 10 and 30 min

Aggregation kinetic of citrate synthase (32 ug/mL) in 10 mM Tris-HCl buffer at pH 7.2, was studied by observing changes in optical density (OD) at 360 nm for 60 min at 45 °C, first with CS only as a control, and after in presence of $Au_{25}(SG)_{18}$ nanoclusters (120 µg/mL) added at 10 and 30 min after starting the measurement. Optical density was observed on a Varian Cary 50 spectrophotometer whose temperature is controlled with a Thermomix 1460 recirculating heater, using a quartz cuvette of 10 mm path length. Tris-HCl buffer solution was pre-heated for 8 min until reaching 45 °C in absence of CS before the assay.

2.9. Dynamic light scattering (DLS)

The influence of Au NCs and temperature on the hydrodynamic radius (R_h) of citrate synthase and aldolase during aggregation were evaluated by DLS measurements carried out on a Zetasizer Nano (Malvern Panalytical). Size measurement of citrate synthase (27 ug/mL) without and in presence of $Au_{25}(SG)_{18}$ (25.7 and 102.8 µg/mL) was carried out in 10 mM Tris-HCl buffer pH 7.2 at 45 °C for 60 min, and size measurement of aldolase (130 µg/mL) without and in presence of $Au_{25}(SG)_{18}$ (107.1 and 312.4 µg/mL) was carried out in 50 mM Phosphate buffer pH 7.2 at 60 °C for 18 min.

2.10. Absorption spectra

All UV-vis spectra were monitored by a Varian Cary 50 spectrophotometer. UV-vis spectra of nanoclusters were analyzed from 250 – 900 nm in Milli-Q water using a quartz cuvette of 10 mm path length. Full UV-vis spectra of protein-nanoclusters conjugation were analyzed from 200 – 900 nm wavelength, after 60 min thermal aggregation of proteins (CS

and BSA) in absence and in presence of nanoclusters according description in section 2.5 and 2.7 using a quartz cuvette of 10 mm path length. Samples after thermal aggregation were placed immediately in ice bath to stop aggregation of proteins before measuring full UV-vis spectrum. Infrared spectrum of 3-MBA nanocluster was measured using Biorad Excalibur FTIR-spectrometer equipped with a Specac Golden Gate ATR with diamond crystal, the sample was dissolved in minimum amount of Milli-Q water and was dropped on the ATR crystal window to form a thin film of NC and dried at room temperature before measurement.

3. Results

3.1. Synthesis of Au NCs

$Au_{25}(SG)_{18}$ nanoclusters were synthesized according to the literature procedure,[4] at room temperature and ambient conditions, using a single-steps synthesis technique which includes two reduction steps until obtaining Au(0) as was detailed in the synthesis procedure in chapter 2. UV-vis absorbance spectroscopy confirmed the synthesis of $Au_{25}(SG)_{18}$ nanoclusters. The spectrum showed absorption bands at 450 and 670 nm, with two weak shoulder peaks around 340 and 400 nm (Figure 14), which are characteristic absorption bands for $Au_{25}(SG)_{18}$ nanoclusters and are in good agreement with the literature.[4, 25]

The synthesis of $Au_{25}(Capt)_{18}$ was confirmed by using UV-vis absorbance spectroscopy and following the synthesis method proposed by Roy et al.[26] Briefly, gold salt ($HAuCl_4$) first reacts with excess thiol to form gold-thiolate Au(I)Capt aggregate complexes, then, $NaBH_4$ is added to reduce Au(I)Capt to $Au_{25}(Capt)_{18}$ nanoclusters. The UV-vis spectrum shows absorption bands at 450 and 670 nm, and two weak absorption bands around 400 and 550 nm (Figure 15). These absorption bands were in accordance with those showed in the literature. [2, 26]

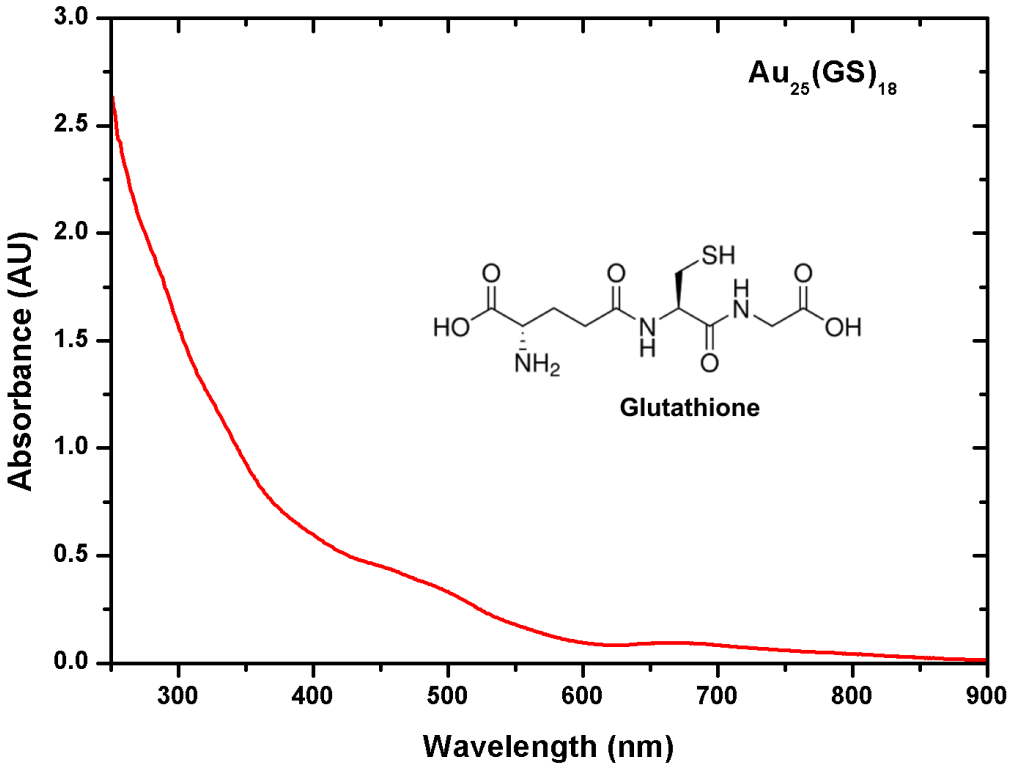

Figure 14. UV-vis absorption spectrum of $Au_{25}(SG)_{18}$ nanoclusters.

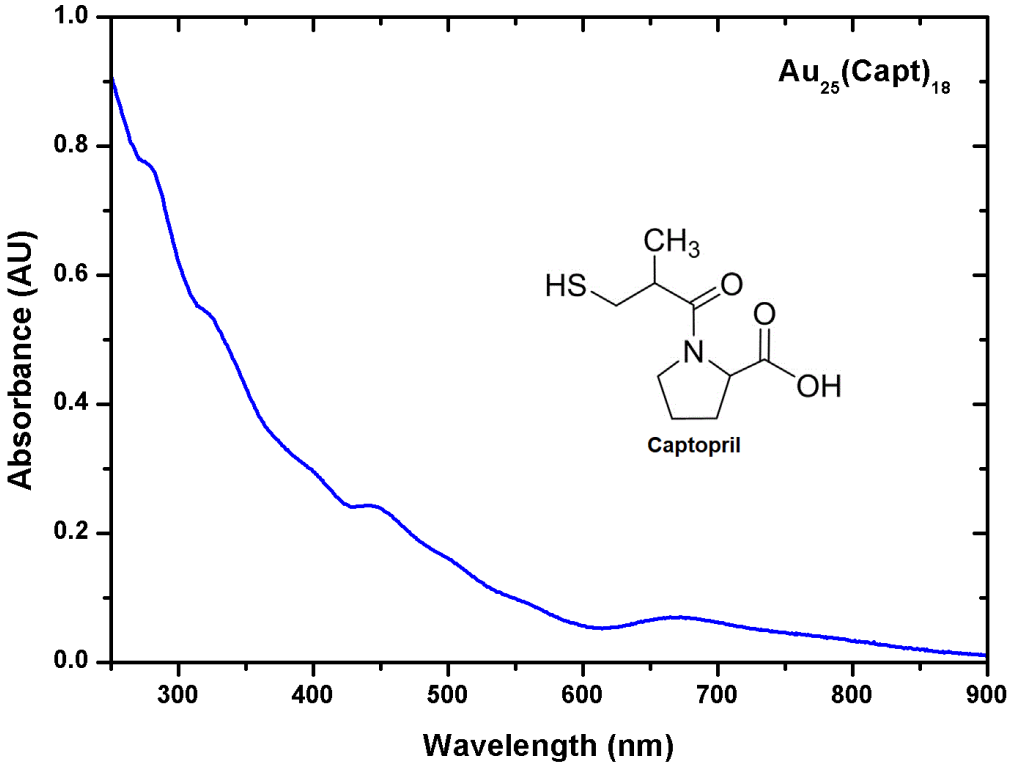

Figure 15. UV-vis absorption spectrum of $Au_{25}(Capt)_{18}$ nanoclusters.

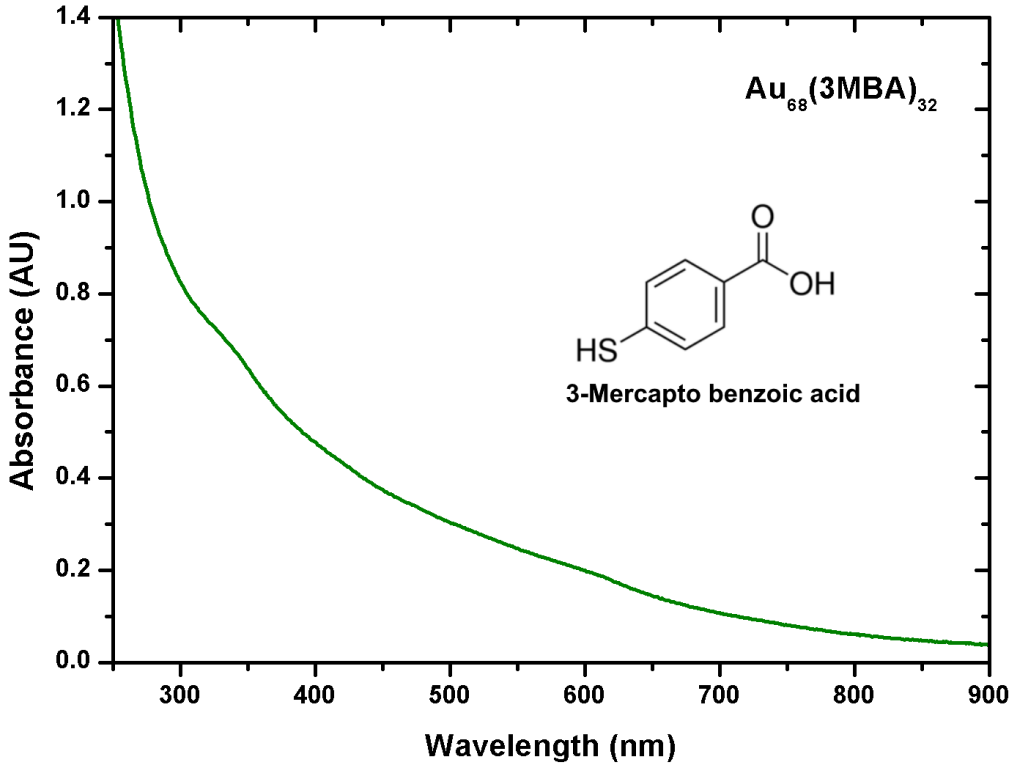

Figure 16. UV-vis absorption spectrum of $Au_{68}(3\text{-MBA})_{32}$ nanoclusters.

In the case of $Au_{68}(3\text{-MBA})_{32}$, the synthesis was made in accordance to the procedure published by Azubel et al.[9] The synthesis is accomplished in two steps, reduction of Au(III) to Au(I) by thiol, and further reduction to Au(0) by borohydride. Two factor factors are critical in the synthesis for obtaining nanoclusters uniform in size: Adjustment of the pH to 13 during first reduction by thiol, and equilibration for about 16h during second reduction by borohydride. UV-vis spectrum of $Au_{68}(3\text{-MBA})_{32}$ was rather featureless (Figure 16), the spectrum did not show any prominent peak as was expected according to the literature.[30] $Au_{68}(3\text{-MBA})_{32}$ was also studied by FTIR spectroscopy, the IR spectrum (Figure 17) showed two prominent peaks below 1800 cm^{-1} surrounded by others minor peaks This pattern was also found in larger Au 3MBA NCs and correspond to the ligand vibration which is not affected by cluster size.[30] The spectrum also presented a broad band around 2000 – 2400 cm^{-1} corresponding to the electronic absorption of Au_{68} nanocluster as was reported in literature.[30] A prominent broad band between 2500 – 3700 cm^{-1} corresponds principally to the contribution of OH stretching vibrations of H_2O. These signals arise because the nanoclusters, previously dissolved in Milli-Q water, were dropped cast over the ATR crystal and dried at room temperature before measurement.

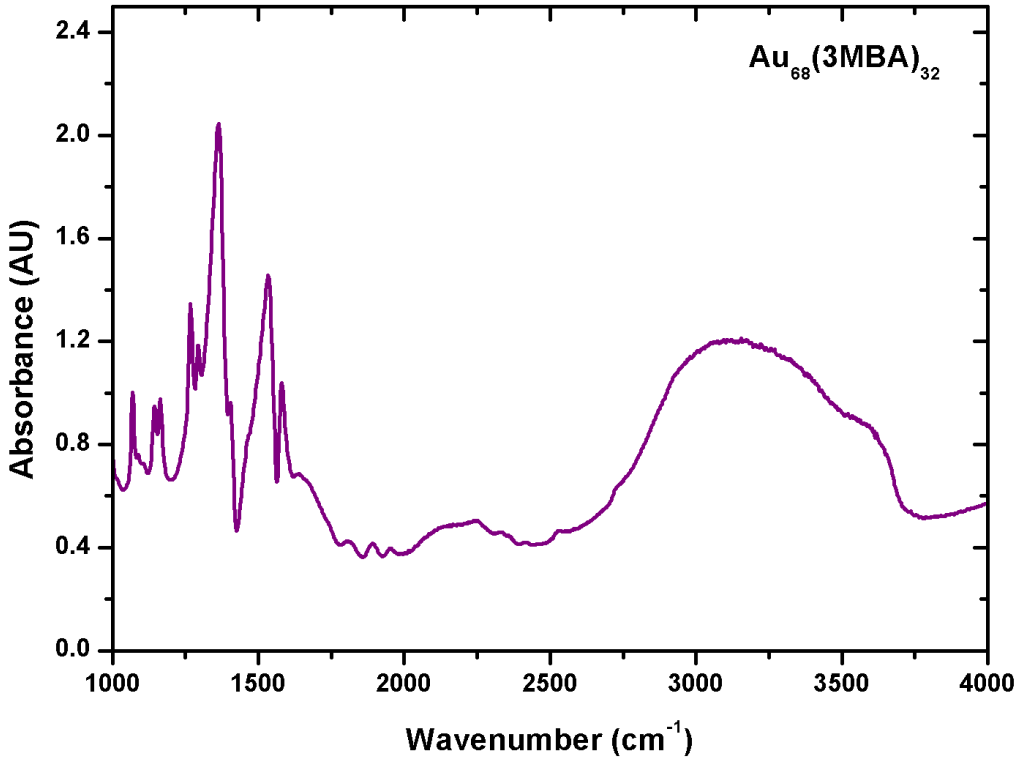

Figure 17. IR spectrum of Au_{68}(3-MBA)$_{32}$ nanoclusters.

3.2. Thermal aggregation of citrate synthase

Optical density (OD) is most accurate and time saving measurement for biomass concentration when light attenuation is dominated by scattering. In suspensions containing mixture of two or more phases, light is scattering due to difference in refractive index and contribute to light attenuation.[77] Protein aggregation was facilitated by thermal stress, which disturbs protein stability and results in the formation of high molecular weight aggregates. These particles render the protein solution turbid because they scatter light.[45] Heat-induced aggregation was monitored by optical density (OD) and by dynamic light scattering (DLS). The first shows the level of aggregating particle formation, and the second gives us the hydrodynamic diameter of those aggregates formed over the time. As Au NCs absorb light in the UV-vis spectrum and can interfere in the OD measuring, the OD was set to zero at the beginning of each experiment (t= 0 min), this facilitate to study the beginning of the aggregation.

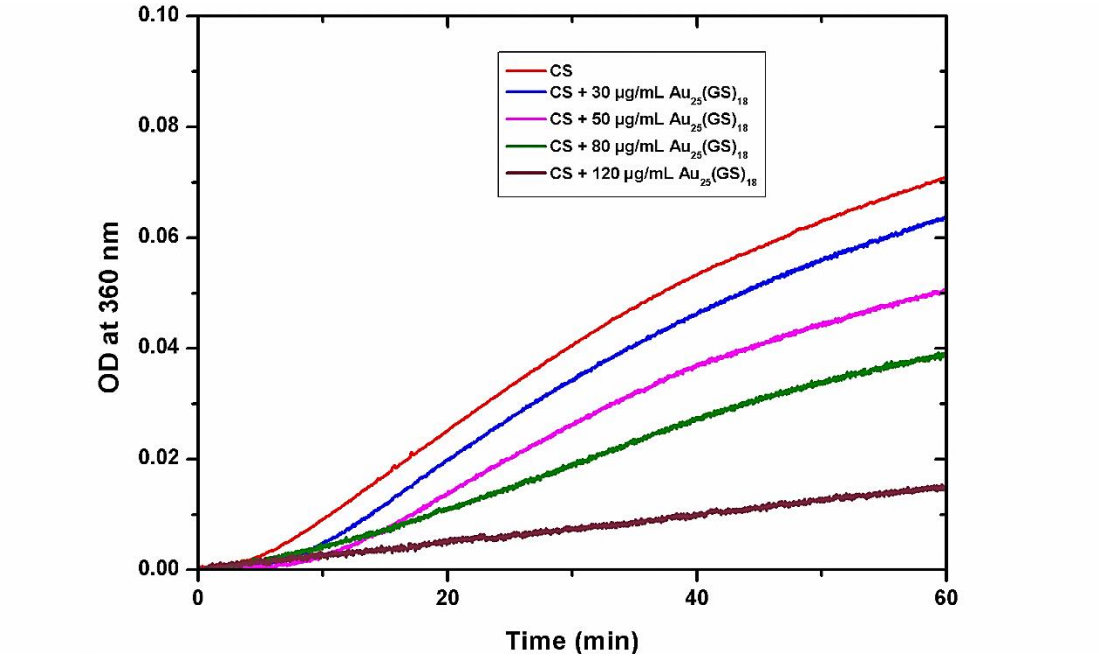

Figure 18. Thermal aggregation of citrate synthase (32 µg/mL) in 10 mM Tris-HCl buffer (pH 7.2) at 45 °C was studied by measuring optical density at 360 nm for 60 min, in absence and with different concentration of $Au_{25}(SG)_{18}$ nanoclusters (30, 50, 80 and 120 µg/mL).

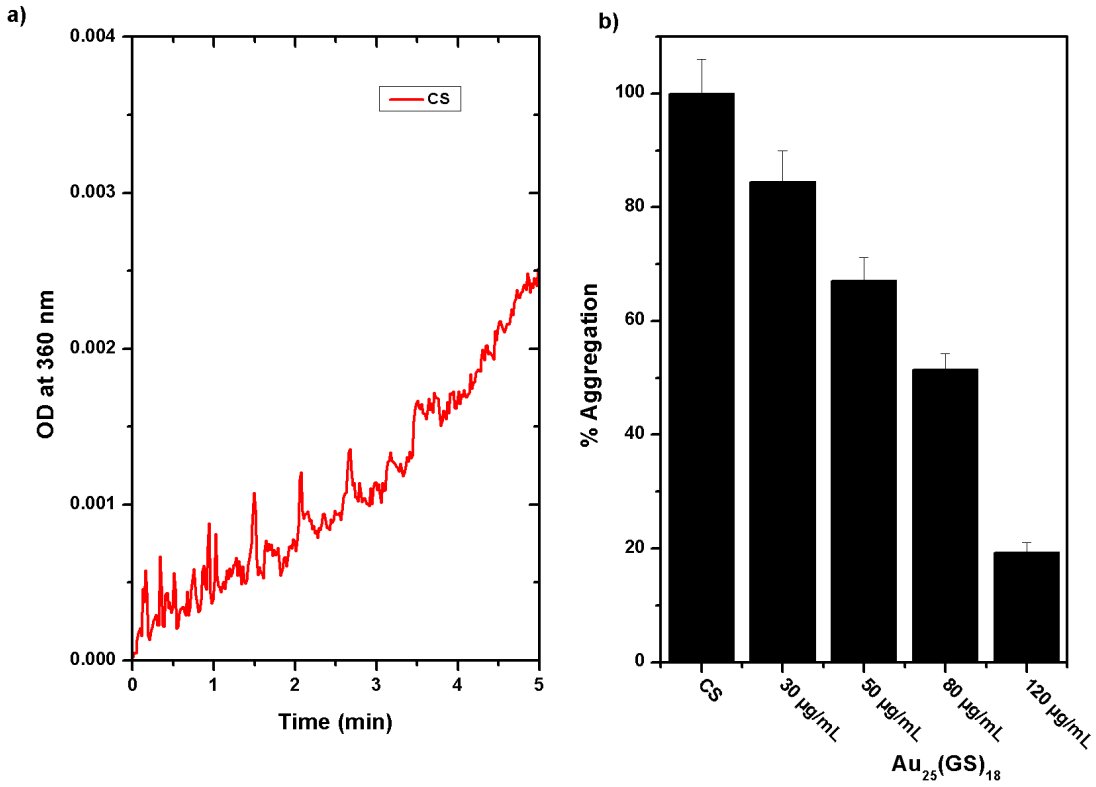

Figure 19. a) OD at 360 nm of the first 5 min during aggregation of CS (32 µg/mL CS in 10 mM Tris-HCl buffer pH 7.2 at 45 °C) **b)** Bar diagram representing percent aggregation of CS for data shown in Figure 18. Standard deviations are represented as error bars.

Aggregation of CS at 45 °C in absence and with different concentration of $Au_{25}(SG)_{18}$ nanoclusters is given in Figure 18. The aggregation of CS (32 µg/mL) in the absence of Au nanoclusters started from the beginning, as is shown in Figure 19a. The aggregation of CS has an initial lag period in which aggregation is slow before ~5 min. This lag period is due to the formation of initial seeds of protein aggregates.[63] The ability of aggregates to seed and further propagate aggregation to other proteins is consistent with the idea that thermal aggregation of proteins includes the stage of nucleation.[78] After ~5 min, further increasing in size of aggregates is observed and thus, optical density rate also increases rapidly, keeping this rate until completing 60 min. This continuous increase of the turbidity (OD at 360 nm) during 60 min heating at 45 °C confirms the aggregation of CS. The temperature at 45 °C was chosen because the aggregation of CS starts at 43 °C and this temperature is widely used in the literature.[45]

The optical density curve of CS solution in presence of the different concentrations of $Au_{25}(SG)_{18}$ nanoclusters were lower compared to the curve of CS in absence of Au NCs. This adds evidences for a possible chaperone like activity of the $Au_{25}(SG)_{18}$ nanoclusters through the reduction of the aggregation rate of CS. This reduction of the aggregation was expressed in percentage in a bar diagram (Figure 19b) as was reported in the literature,[79] in which the final value of the aggregation profile was used for calculation, native protein was taken as 100 % and percent aggregation for other samples were calculated with respect to that native protein. This percentage was also calculated for other proteins aggregation profiles. In presence of 30 µg/mL of $Au_{25}(SG)_{18}$ nanoclusters, the aggregation of CS (32 µg/mL) decreased to 84.5 % and was reduced to 67.2 and 51.5 % in presence of 50 and 80 µg/mL of $Au_{25}(SG)_{18}$ nanoclusters respectively. The aggregation was significantly reduced to 19.4 % when 120 µg/mL of $Au_{25}(SG)_{18}$ nanoclusters were added to the protein solution.

Presumably, native CS proteins under temperature stress unfold and interact with $Au_{25}(GS)_{18}$ nanocluster, which aggregates until saturation. Increasing NCs concentration permits it to interact with more unfolded CS and saturate faster the aggregates, inhibiting further aggregation, this is evidenced with reduction of turbidity (scattering light) and expressed in less OD measurement of samples.

Full UV-vis spectra after thermal treatment of proteins in presence of nanoclusters were also measured. Proteins absorb UV light at 220 nm due to the peptide bonds and also most proteins absorb light at 280 nm, which depends primarily upon the fraction of aromatic amino acids (phenylalanine, tryptophan and tyrosine) within the protein.[80] Full UV-vis spectra of CS after thermal treatment in absence and in presence of GS NCs are shown in Figure 20. Absorption bands at 670 and 450 nm corresponding to $Au_{25}(SG)_{18}$ nanoclusters were distinguished and came prominent when its concentration was increased. Other peaks around 220 and 280 nm corresponding to CS were also distinguished. Both peaks were red shifted (~20 nm) and would be due to the combined contribution from protein and nanoclusters and/or a possible interaction between them.

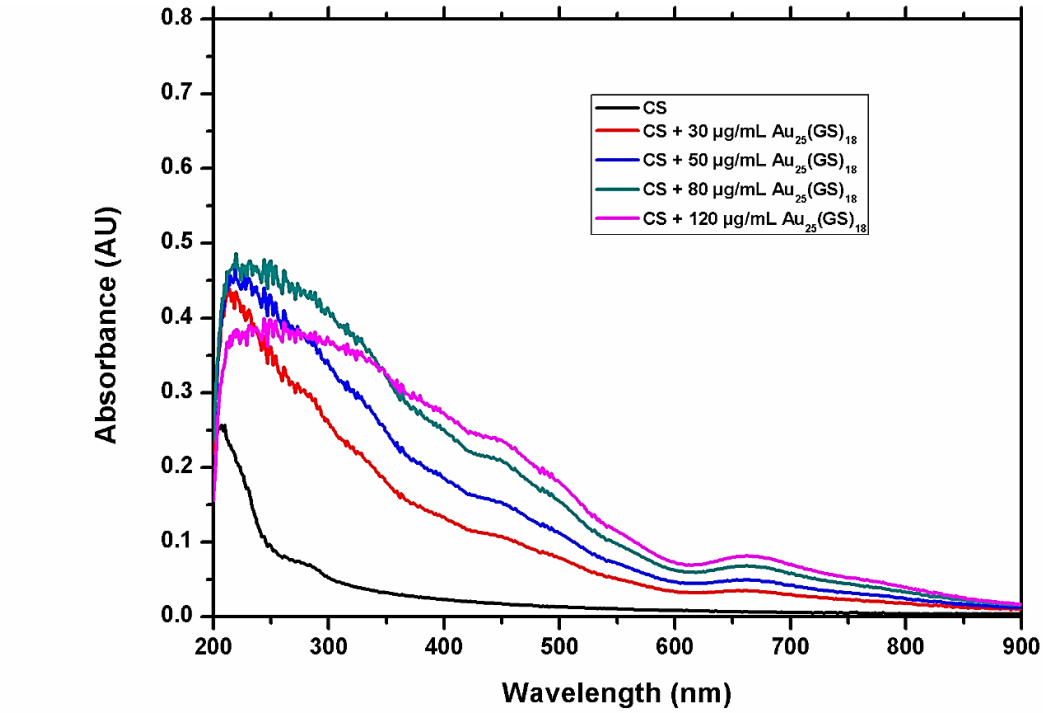

Figure 20. Full UV-vis spectra (200 – 900 nm) of CS (32 µg/mL) in 10 mM Tris-HCl buffer (pH 7.2) measured after 60 min thermal treatment (45 °C) in absence and in presence of $Au_{25}(SG)_{18}$ (30, 50, 80 and 120 µg/mL).

Aggregation of CS (32 µg/mL) in presence of $Au_{25}(Capt)_{18}$ nanoclusters also at 45 °C (Figure 21) showed similar effect than in presence of $Au_{25}(SG)_{18}$, with 30 µg/mL of $Au_{25}(Capt)_{18}$, the aggregation of CS decreased to 79.9 %, and subsequently to 64.7 and 43.9 % in presence of 50 and 80 µg/mL of captopril nanoclusters respectively, whereas lowest decreasing (36.1 %) was obtaining with 120 µg/mL nanoclusters, as is shown in Figure 22. Aggregation profile of CS in presence of captopril and glutathione nanoclusters were similar (difference less than ~7.6 %) at same concentrations (30, 50 and 80 µg/mL), but in presence of higher concentration of Au NCs (120 µg/mL), $Au_{25}(SG)_{18}$ seems to be

more effective in reducing aggregation of CS, 16.7 % higher reduction than $Au_{25}(Capt)_{18}$ nanoclusters.

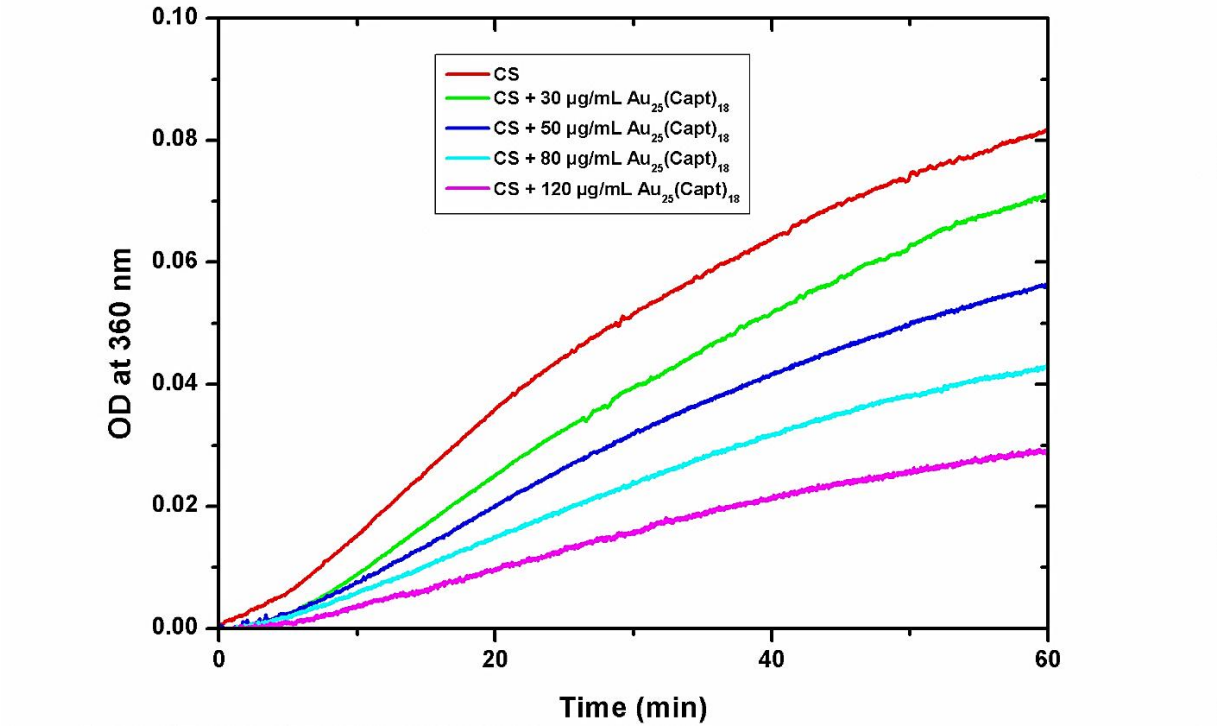

Figure 21. Thermal aggregation of citrate synthase (32 µg/mL) in 10 mM Tris-HCl buffer (pH 7.2) at 45 °C was studied by measuring optical density at 360 nm for 60 min, in absence and with different concentration of $Au_{25}(Capt)_{18}$ nanoclusters (30, 50, 80 and 120 µg/mL).

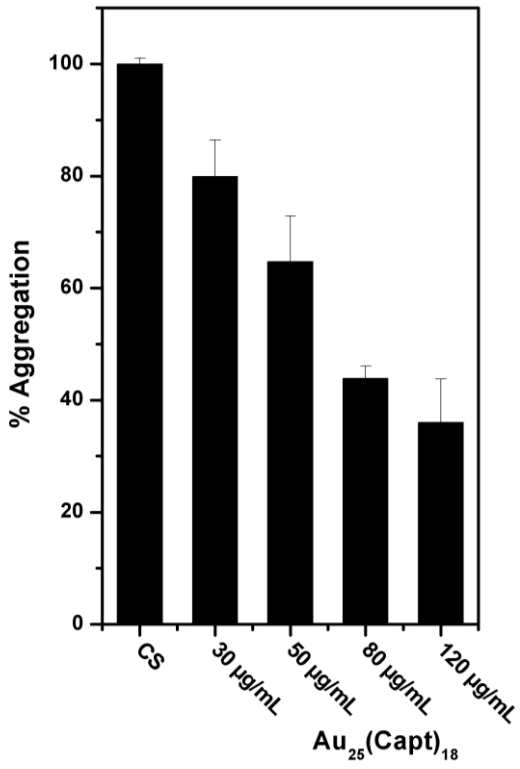

Figure 22. Bar diagram representing percent aggregation of CS in absence and presence of 30, 50, 80 and 120 µg/mL of $Au_{25}(Capt)_{18}$. Standard deviations are represented as error bars.

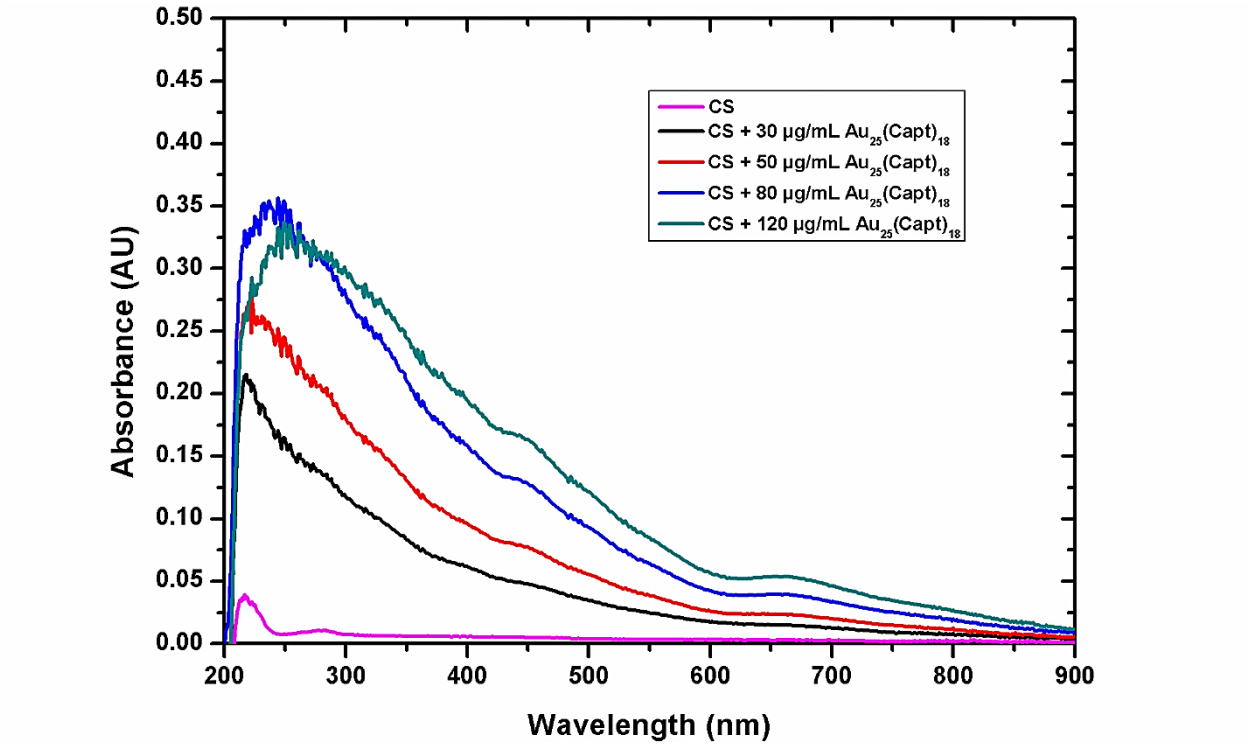

Figure 23. Full UV-vis spectra (200 – 900 nm) of CS (32 µg/mL) in 10 mM Tris-HCl buffer (pH 7.2) measured after 60 min thermal treatment (45 °C) in absence and presence of $Au_{25}(Capt)_{18}$ (30, 50, 80 and 120 µg/mL).

Full UV-vis spectra of CS in presence of $Au_{25}(Capt)_{18}$ nanoclusters (Figure 23) showed absorption bands at 450 and 670 nm corresponding to the nanoclusters, which were intensified when concentration increased, and peaks around 220 and 280 nm belonging to CS, gradually disappeared due to high contribution of UV absorption of Capt NCs.

Aggregation of CS in presence of $Au_{68}(3MBA)_{32}$ nanoclusters was also studied at 45 °C (Figure 24). Concentration of CS was the same as in previous aggregating experiments (32 µg/mL), but the concentration of 3MBA NCs used were notably lower than those used with Capt and GS NCs, which evidences the better effectiveness of $Au_{68}(3MBA)_{32}$ to reduce aggregation.

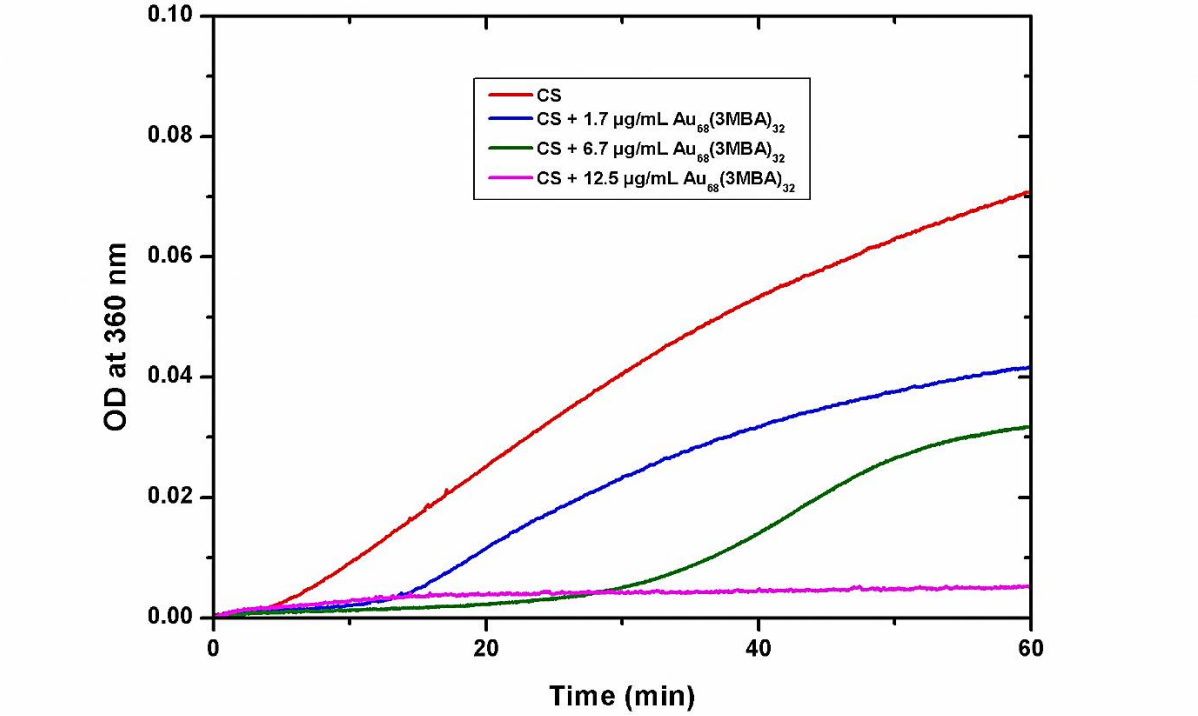

Figure 24. Thermal aggregation of CS (32 µg/mL) in 10 mM Tris-HCl buffer (pH 7.2) at 45 °C was studied by measuring optical density at 360 nm for 60 min, in absence and presence of different concentration of $Au_{68}(3MBA)_{32}$ nanoclusters (1.7, 6.7 and 12.5 µg/mL).

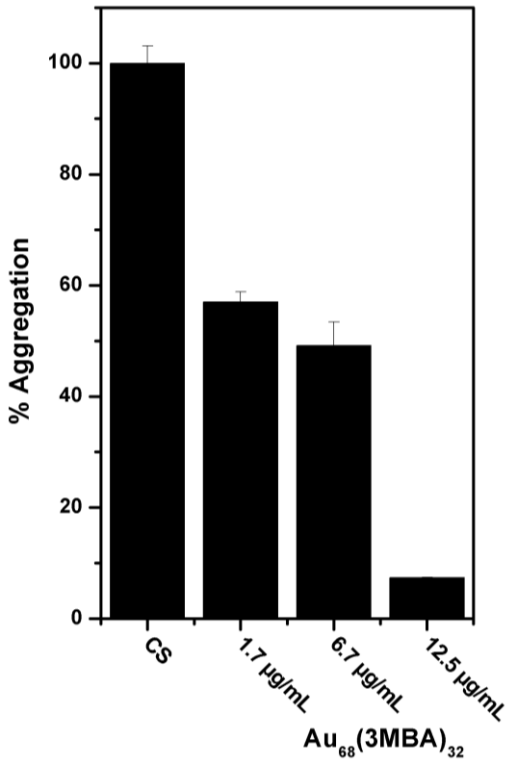

Figure 25. Bar diagram representing percent aggregation of CS in absence and presence of 1.7, 6.7 and 12.5 µg/mL of $Au_{25}(3MBA)_{18}$ nanoclusters. Standard deviations are represented as error bars.

As was explained before, aggregation of CS has an initially lag period in which formation of initial seeds of proteins aggregates happened (nucleation stage). This lag period in the aggregation of CS in presence of 3MBA NCs was extended when increasing concentration of nanoclusters, and as consequence retards propagation of protein aggregation. This phenomenon suggests interactions of unfolded CS with $Au_{68}(3MBA)_{32}$ during initial nucleation state. Rapid propagation of aggregation of CS started at ~13 and ~30 minutes for 1.7 and 6.7 µg/mL of 3MBA NCs respectively. When using 12.5 µg/mL of 3MBA NCs the rate of aggregation kept low. Percent aggregation of CS was reduced to 57.0 % and 49.2 % in presence of 1.7 and 6.7 µg/mL of $Au_{68}(3MBA)_{32}$ nanoclusters. The aggregation was significantly reduced to 7.4 % when 12.5 µg/mL of $Au_{68}(3MBA)_{32}$ nanoclusters were used (Figure 25).

A comparison diagram of percent aggregation of CS in absence and presence of each nanocluster ($Au_{25}(SG)_{18}$, $Au_{25}(Capt)_{18}$ and $Au_{25}(3MBA)_{18}$) is shown in Figure 26.

Full UV-vis spectra of CS in presence of $Au_{68}(3MBA)_{32}$ nanoclusters after thermal treatment were analyzed (Figure 27) and showed two peaks at 220 and 280 nm (corresponding to the CS) followed with a featureless spectrum profile as expected for $Au_{68}(3MBA)_{32}$. The peak at 280 nm was more prominent when concentration of nanoclusters increased but it kept at same wavelength. However, the peak at 220 nm was red shifted (~10 nm) probably due to a possible CS-nanocluster interaction and/or UV absorption contribution of nanocluster.

Additionally, experiments were performed where $Au_{25}(SG)_{18}$ nanoclusters were added to CS after 10 and 30 min (Figure 28) to study the effect of NCs after initial protein aggregation. Results showed that nanoclusters can still inhibit the aggregation of proteins even though the protein initially aggregated for 10 and 30 min, respectively. This protective nature of NCs towards protein can be explained by the interaction of NCs with unfolded proteins avoiding them to further aggregate, similar to the properties of holding chaperones. Hence water soluble nanoclusters also possess the holdase activity i.e. NCs bind to the unfolded proteins and prevent them from further aggregating.[81]

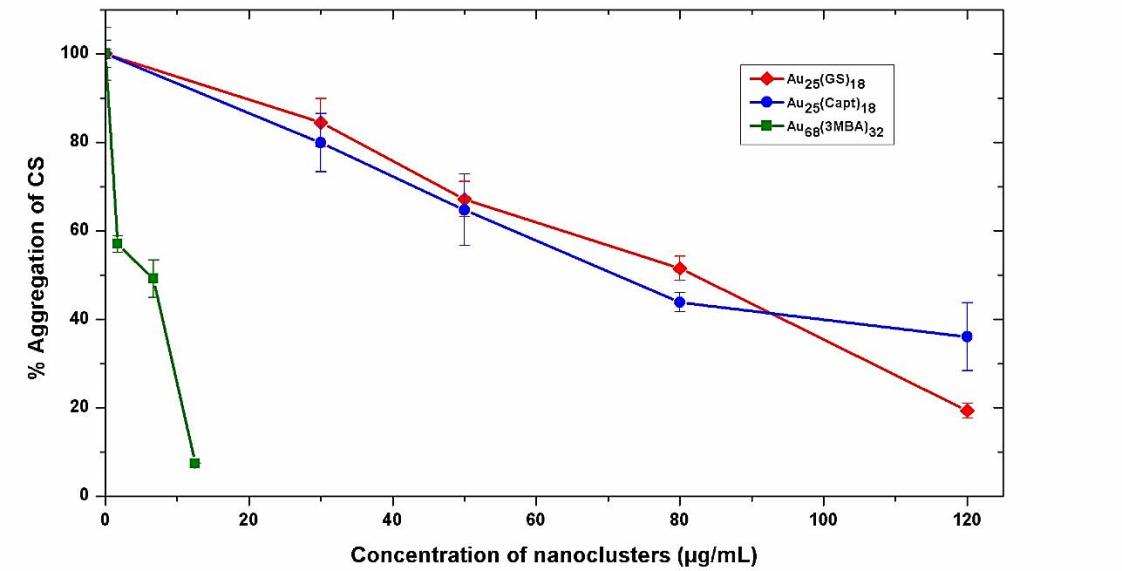

Figure 26. Percent aggregation of CS in absence and presence of $Au_{25}(SG)_{18}$, $Au_{25}(Capt)_{18}$ and $Au_{25}(3MBA)_{18}$ nanoclusters. Standard deviations are represented as error bars.

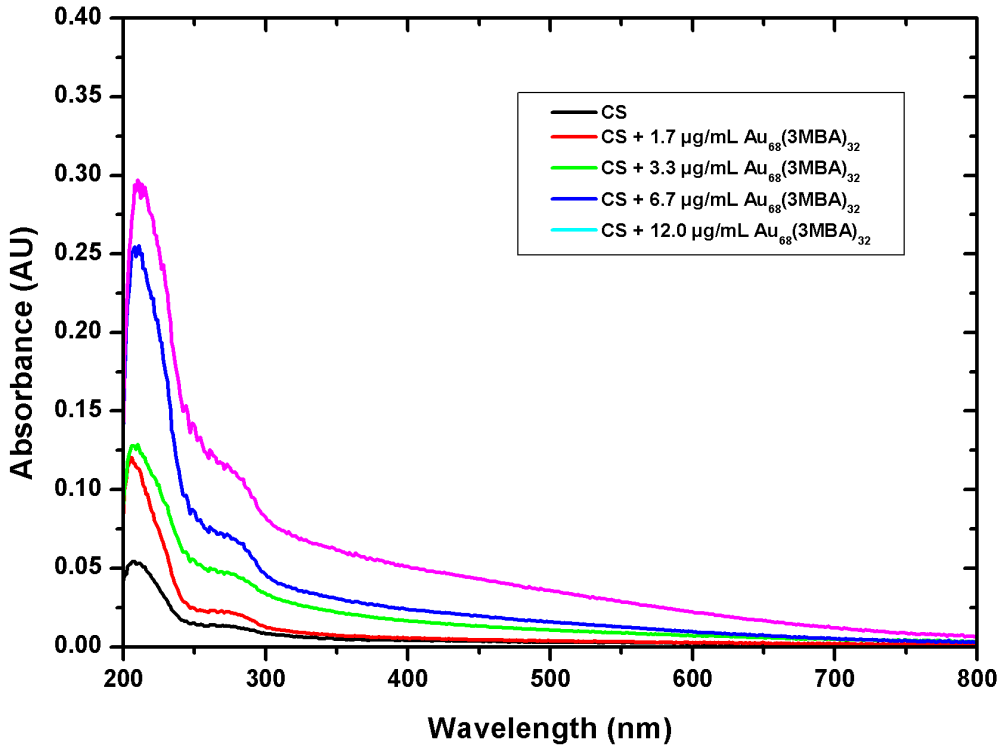

Figure 27. Full UV-vis spectra (200 – 900 nm) of CS (32 µg/mL) in 10 mM Tris-HCl buffer (pH 7.2) measured after 60 min thermal treatment (45 °C) in absence and presence of $Au_{68}(3MBA)_{32}$ nanoclusters (1.7, 3.3, 6.7 and 12.0 µg/mL).

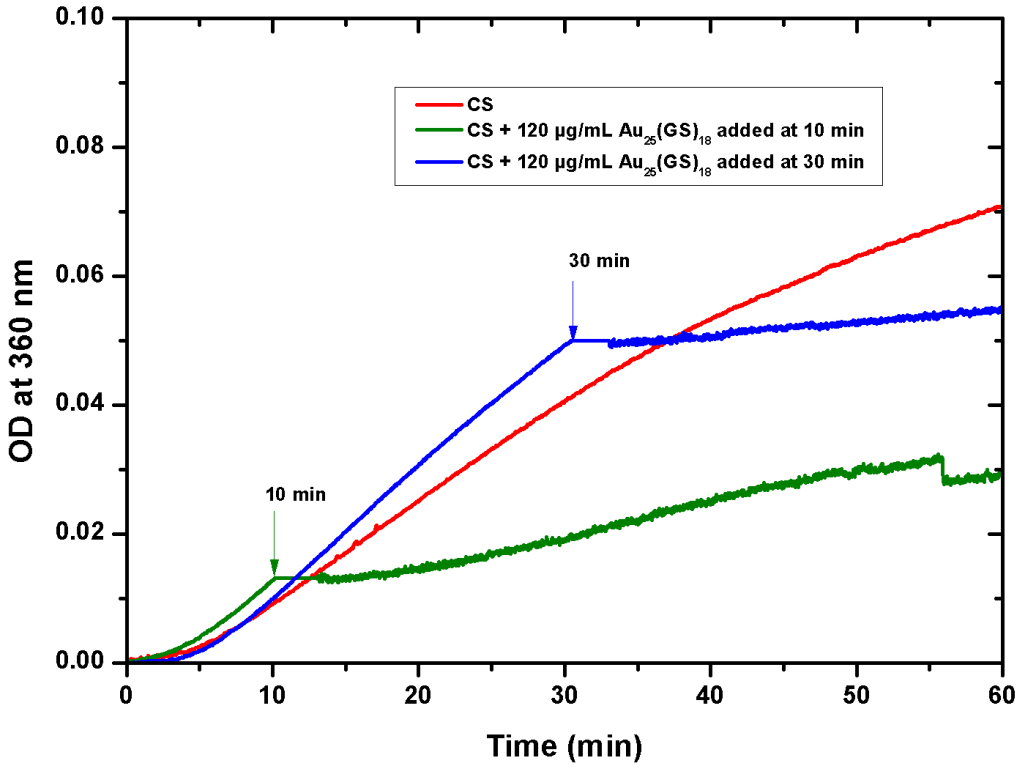

Figure 28. Thermal aggregation of CS (32 µg/mL) in 10 mM Tris-HCl buffer (pH 7.2) at 45 °C was studied by measuring optical density at 360 nm for 60 min, in absence and presence of 120 µg/mL of $Au_{25}(SG)_{18}$ nanoclusters added after 10 and 30 min.

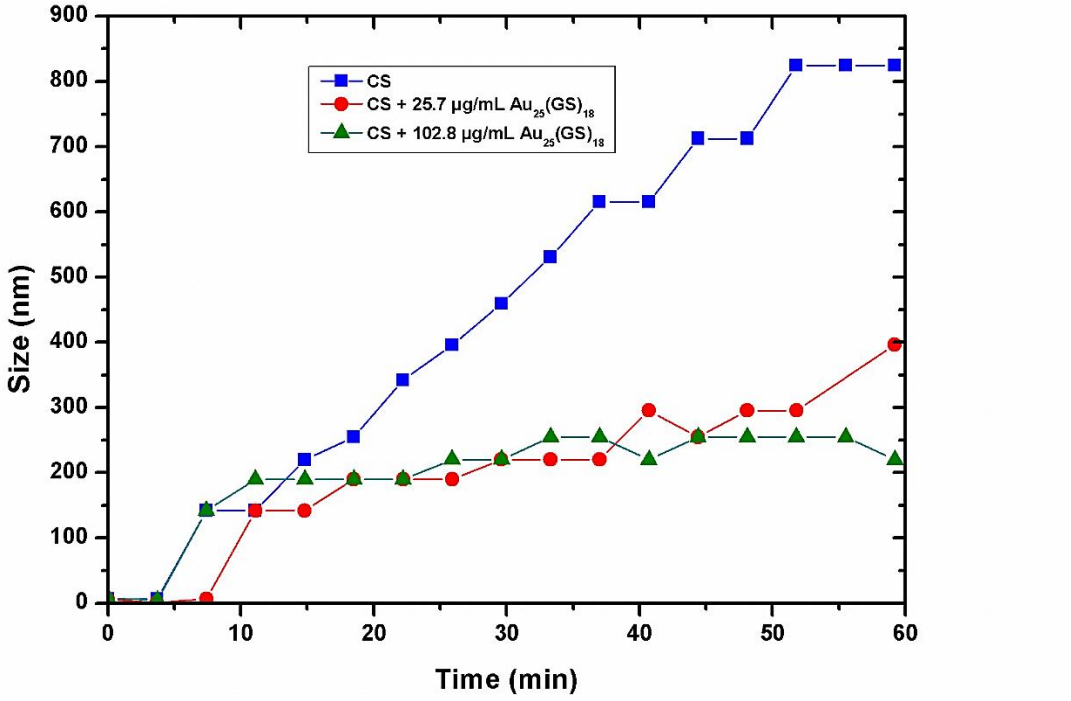

Figure 29. DLS of citrate synthase (27 µg/mL) in 10 mM Tris-HCl buffer (pH 7.2) at 45 °C was measured for 60 min, in absence and presence of different concentration of $Au_{25}(SG)_{18}$ nanoclusters (25.7 and 102.8 µg/mL).

DLS measurements were done to study the hydrodynamic diameter evolution of aggregates during thermal aggregations of CS in presence of $Au_{25}(SG)_{18}$ nanoclusters. As it is shown in Figure 29, aggregation of CS started slowly at the beginning and after ~4 min size of aggregates increased rapidly (blue line) and followed the same growth kinetics until 60 min where the size of the aggregates reached 825 nm. In presence of 25.7 µg/mL of GS NCs, size of aggregates increases rapidly until reaching 190 nm after 7 min. After that the growth kinetics was reduced drastically. After 60 min the aggregate size reached 296 nm. In presence of 102.8 µg/mL of GS NCs, the pattern was similar to 25.7 µg/mL of GS NCs as discussed previously. The aggregates of CS in presence of 102.8 µg/mL shows rapid increase in aggregate size until the size reaches 190 nm at ~11 min and afterwards the kinetics of growth of formation of aggregates slows down. After 60 min the size of the aggregates reached 255 nm.

3.3. Thermal aggregation of aldolase

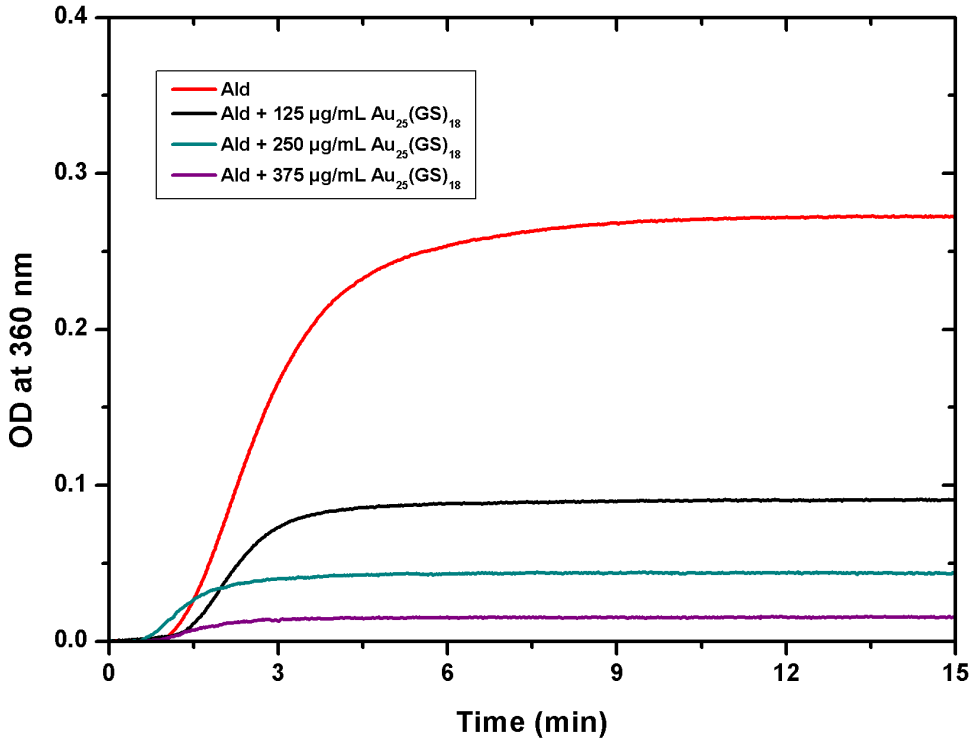

Figure 30. Thermal aggregation of aldolase (150 µg/mL) in 50 mM phosphate buffer (pH 7.2) at 60 °C was studied by measuring optical density at 360 nm for 15 min, in absence and with different concentration of $Au_{25}(SG)_{18}$ nanoclusters (125, 250 and 375 µg/mL).

Aggregation of aldolase at 60 °C was measured in absence and presence of different concentration of $Au_{25}(SG)_{18}$ nanoclusters (Figure 30) and was monitored by turbidity measurement (OD at 360 nm). Aggregation at 60 °C for aldolase was chosen because its aggregation at this temperature was reported successfully in the literature.[82] The

aggregation of aldolase (150 µg/mL) started slowly at the beginning as is shown in Figure 31a. The initial nucleation state lasted 1.2 min, from which propagation of aggregation promote fast size growing of aggregates until ~6 min and continue with a slow increment until 60 min. Aggregation profile was reduced when increasing concentration of $Au_{25}(SG)_{18}$ nanoclusters. This behavior is represented in percentage with respect to the aggregation of native protein using a bar diagram (Figure 31b).

In presence of 125 µg/mL of $Au_{25}(SG)_{18}$ nanoclusters, the aggregation of aldolase decreased significantly to 50.3 %, and was reduced to 26.7 % when adding 250 µg/mL of nanoclusters. The highest reduction of aggregation to 3.9 % was obtained when 375 µg/mL of glutathione nanoclusters were used. $Au_{25}(SG)_{18}$ significantly affected the aggregation profile of aldolase, which suggest an interaction between the protein and GS NCs, this interaction seems to happen from the beginning (nucleation state).

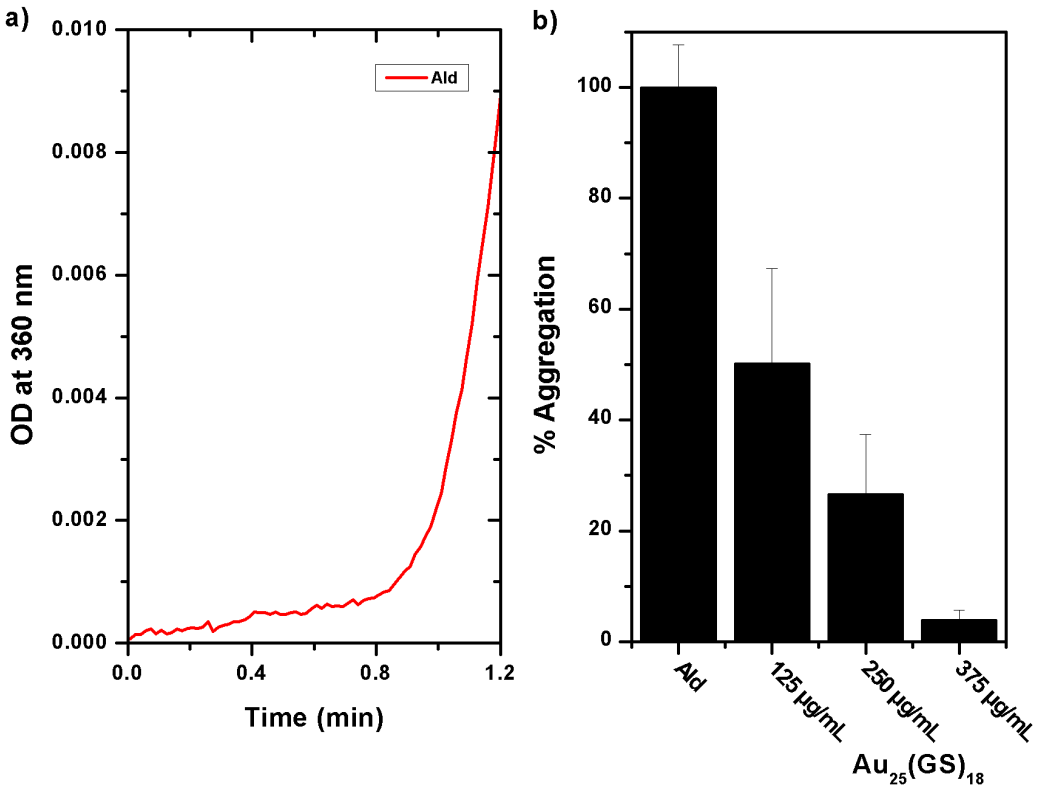

Figure 31. a) OD at 360 nm of the first 1.2 min during aggregation of aldolase (150 µg/mL of aldolase in 50 mM phosphate buffer pH 7.2 at 60 °C) **b)** Bar diagram representing percent aggregation of aldolase for data shown in Figure 30. Standard deviations are represented as error bars.

Further experiments were made to study aggregations of aldolase in presence of $Au_{25}(Capt)_{18}$ nanoclusters (Figure 32). The effect of Capt NCs in aggregation of aldolase was similar to the one described above for GS NCs. Aggregation rate was reduced when

increasing concentration of $Au_{25}(Capt)_{18}$ nanoclusters. Considering aggregation of native protein as 100 %, percentage for others samples was calculated and represented in a bar diagram (Figure 33). Aggregation of aldolase in presence of 50 and 125 µg/mL of $Au_{25}(Capt)_{18}$ nanoclusters decreased to 62,7 and 29.0 % respectively, and in presence of higher concentration of NCs (250 µg/mL), the aggregation decreased drastically to 3.9 %.

A comparison between the aggregation of aldolase in presence of identical concentrations of $Au_{25}(GS)_{18}$ and $Au_{25}(Capt)_{18}$ (125 and 250 µg/mL) showed apparently more effectiveness of Capt NCs to inhibit aggregation than GS NCs (difference of more than 21 %).

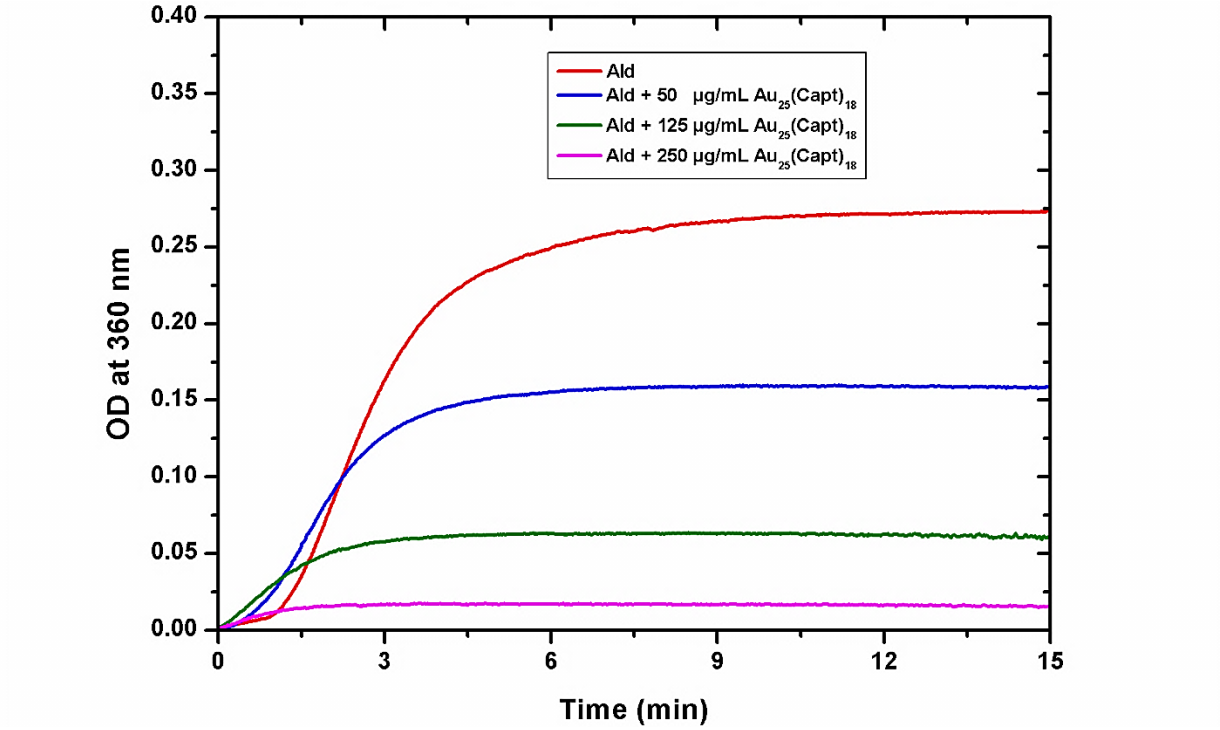

Figure 32. Thermal aggregation of aldolase (150 µg/mL) in 50 mM phosphate buffer (pH 7.2) at 60 °C was studied by measuring optical density at 360 nm for 15 min, in absence and with different concentration of $Au_{25}(Capt)_{18}$ nanoclusters (50, 125 and 250 µg/mL).

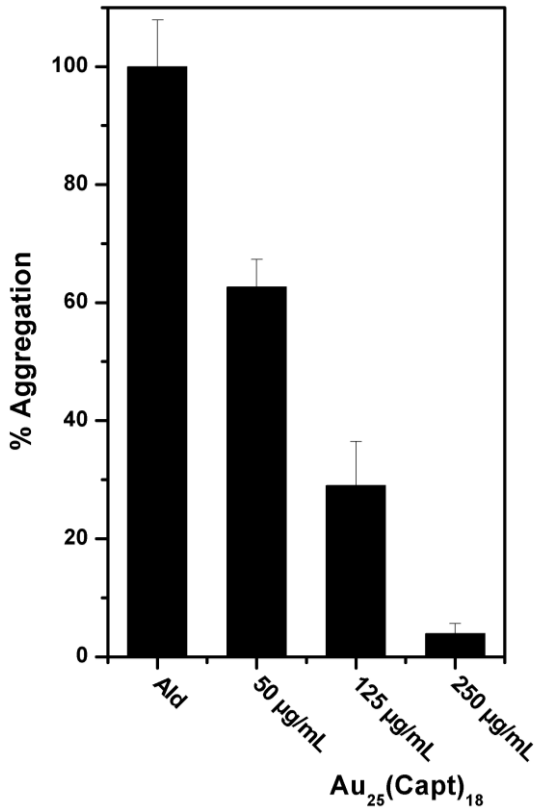

Figure 33. Bar diagram representing percent aggregation of aldolase in absence and in presence of 50, 125 and 250 µg/mL of $Au_{25}(Capt)_{18}$ nanoclusters. Standard deviations are represented as error bars.

Aggregation of aldolase in absence and in presence of $Au_{25}(3MBA)_{18}$ nanoclusters were also measured (Figure 34). Aggregation profile of native aldolase was also affected in presence of nanoclusters, when increasing concentration of 3MBA NCs aggregation profile was reduced. Initial lags (nucleation state) seem not to be affected significantly in presence of 16.7 and 25.0 µg/mL of nanoclusters, but it was drastically increased when using 33.4 µg/mL, probably due to high concentration of 3MBA NCs, which formed abundant protein-NCs conjugates in the nucleation state and retarded drastically the beginning of aggregation.

Aggregation profile in presence of different concentrations of $Au_{25}(3MBA)_{18}$ nanoclusters was also calculated in percentage with respect to the aggregation of native state and was represented in a bar diagram (Figure 35). When aggregation was carried out in presence of 16.7 and 25.0 µg/mL of $Au_{25}(3MBA)_{18}$ nanoclusters, the aggregation was reduced to 66.8 and 46.2 % respectively. Furthermore, a significant reduction of aggregation to 3.1 % was observed when 33.4 µg/mL of nanoclusters were used.

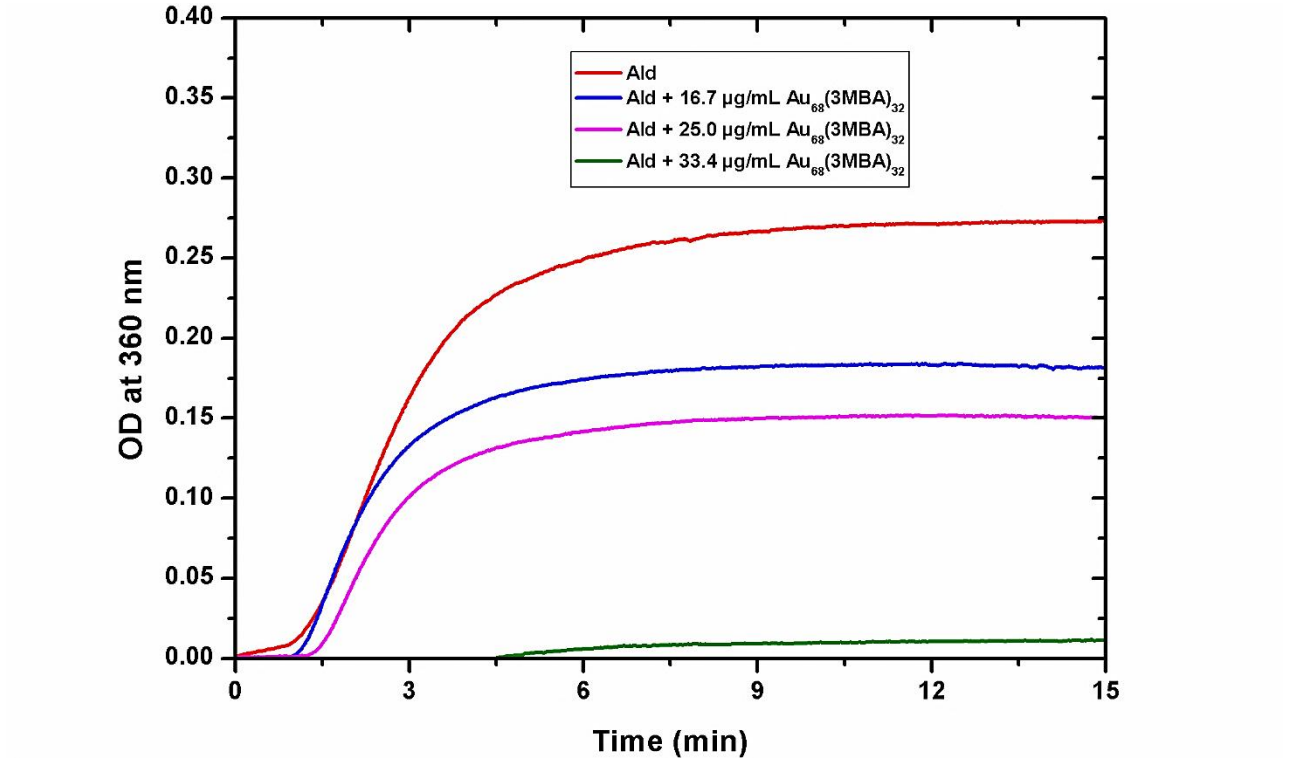

Figure 34. Thermal aggregation of aldolase (150 µg/mL) in 50 mM phosphate buffer (pH 7.2) at 60 °C was studied by measuring optical density at 360 nm for 15 min, in absence and with different concentration of $Au_{68}(3MBA)_{32}$ nanoclusters (16.7, 25 and 33.4 µg/mL).

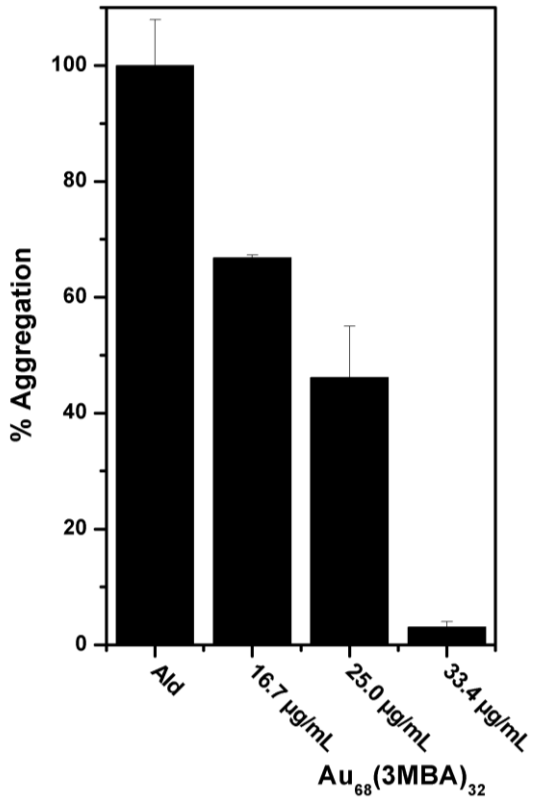

Figure 35. Bar diagram representing percent aggregation of aldolase in absence and in presence of 16.7, 25 and 33.4 µg/mL of $Au_{25}(3MBA)_{18}$ nanoclusters. Standard deviations are represented as error bars.

A comparison diagram of percent aggregation of aldolase in absence and presence of each nanocluster ($Au_{25}(SG)_{18}$, $Au_{25}(Capt)_{18}$ and $Au_{25}(3MBA)_{18}$) is shown in Figure 36.

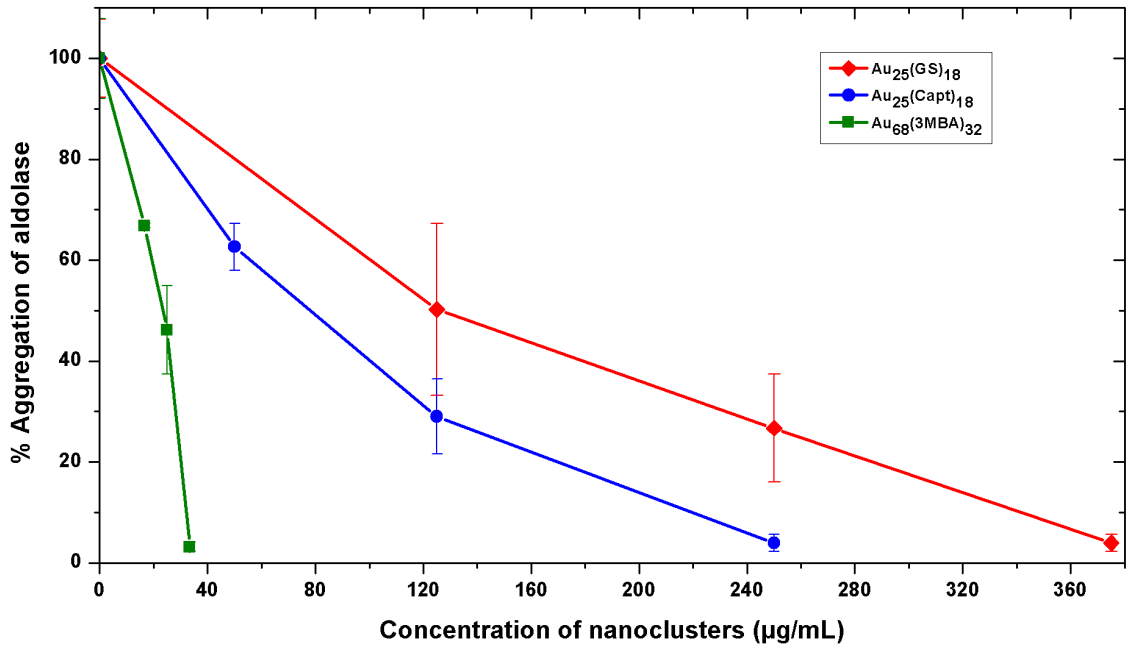

Figure 36. Percent aggregation of aldolase in absence and presence of $Au_{25}(SG)_{18}$, $Au_{25}(Capt)_{18}$ and $Au_{25}(3MBA)_{18}$ nanoclusters. Standard deviations are represented as error bars.

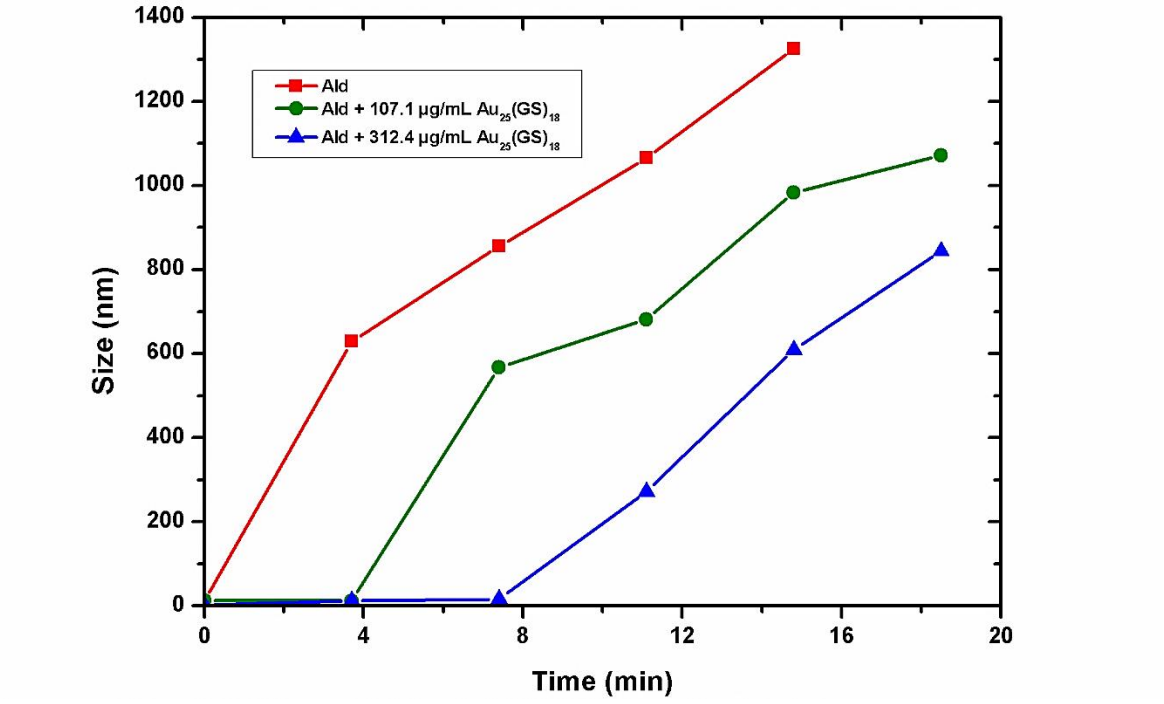

Figure 37. DLS of aldolase (130 µg/mL) in 50 mM phosphate buffer (pH 7.2) at 60 °C was measured for 15 min, in absence and in presence of different concentration of $Au_{25}(SG)_{18}$ nanoclusters (107.1 and 312.4 µg/mL).

DLS measurement was used to study the hydrodynamic diameter of aggregates during thermal treatment of aldolase (60 °C for 15 min) in absence and presence of $Au_{25}(SG)_{18}$ nanoclusters (Figure 37). Size of aggregates when native aldolase was subjected to thermal stress started to increase from the beginning and continued increasing leading to 1326 nm aggregates size at the end of 15 min measurement. Importantly, the aggregation of aldolase in presence of 107.1 and 312.4 µg/mL of nanoclusters, remarkably delay the aggregates formation by 3.4 and 7.4 min respectively, and hence give rise to 609.4 and 983.8 nm size of aggregates respectively at the end of 15 min measurements. Lower size of aggregates in presence of NCs would be due to the interaction of protein with NCs in the nucleation state, these protein-NC conjugates retard formation of seeds and hence overall reduce the size of aggregation.

3.4. Thermal aggregation of BSA

To confirm the effect of Au NCs in protein aggregation, additional experiments using BSA in presence of $Au_{25}(SG)_{18}$ were made (Figure 38), aggregation of native BSA in presence of nanoclusters started rapidly from the beginning as is shown in Figure 39a. When different concentrations of GS NCs were used during aggregation of BSA, the aggregation profile decreased as the concentration of nanoclusters increased, as expected.

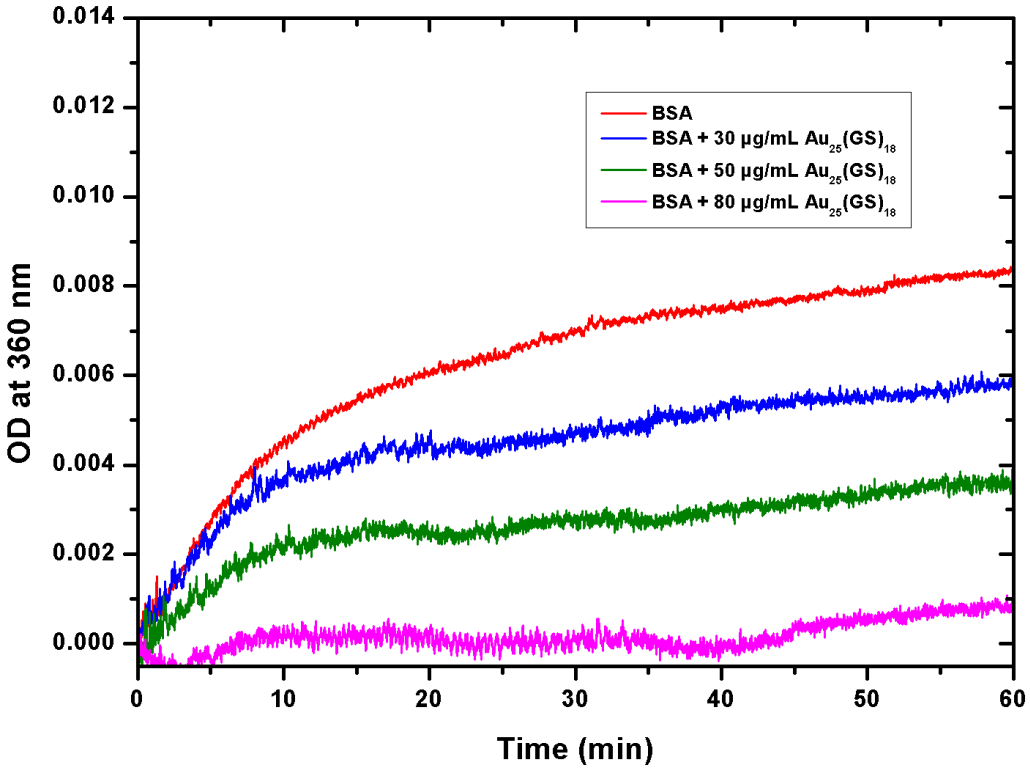

Figure 38. Thermal aggregation of BSA (1 mg/mL) in 10 mM Tris-HCl buffer (pH 7.2) at 70°C was studied by measuring optical density at 360 nm for 60 min, in absence and presence of different concentration of $Au_{25}(SG)_{18}$ nanoclusters (30, 50 and 80 µg/mL).

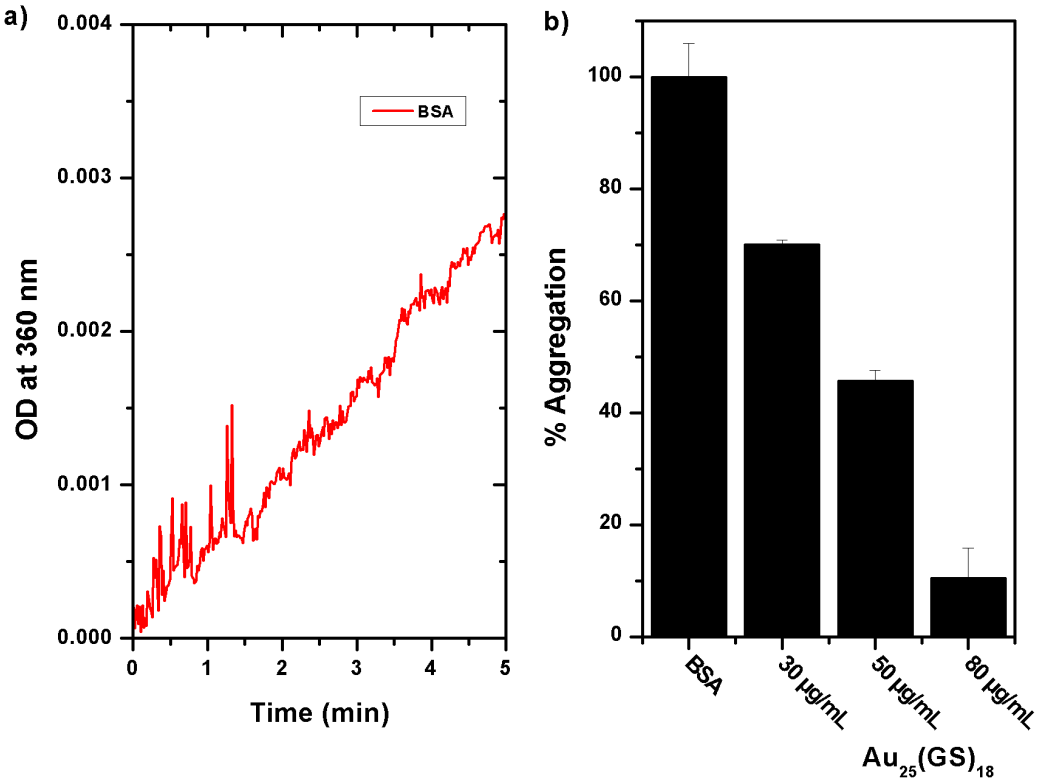

Figure 39. a) OD at 360 nm of the first 5 min during aggregation of BSA (1 mg/mL BSA in 10 mM Tris-HCl buffer pH 7.2 at 70 °C) **b)** Bar diagram representing percent aggregation of aldolase for data shown in Figure 38. Standard deviations are represented as error bars.

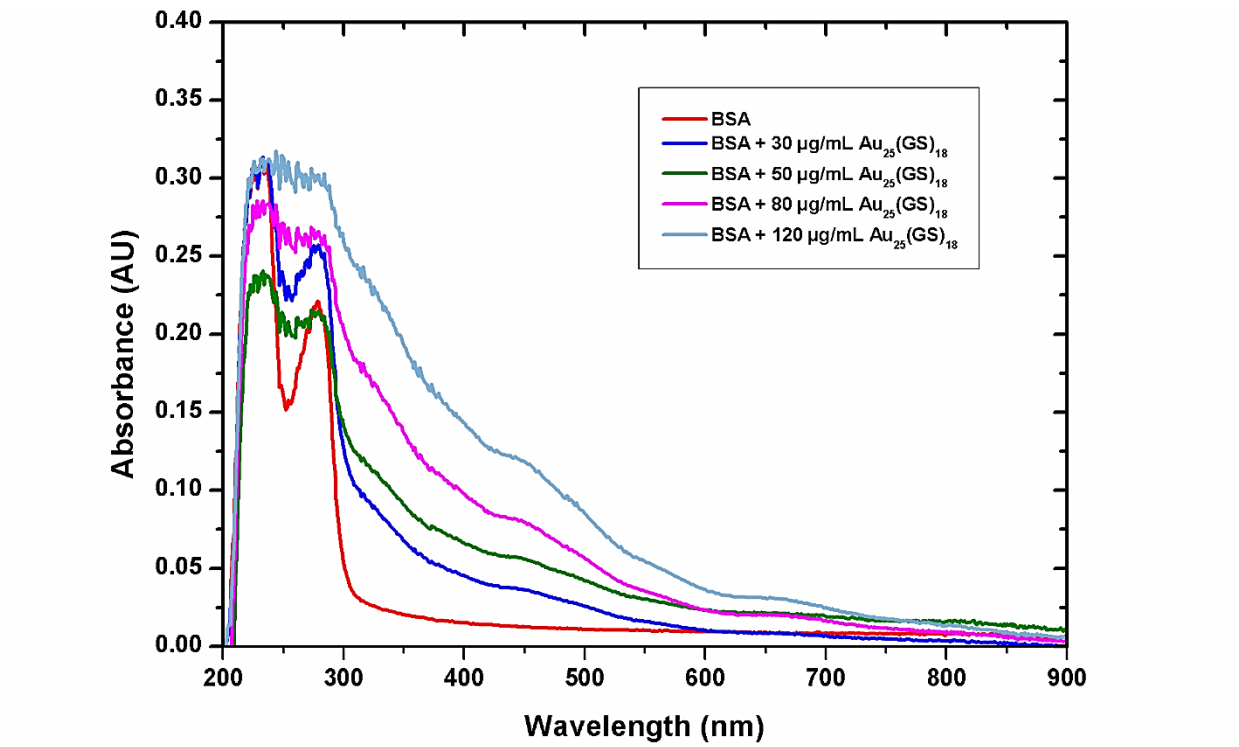

Figure 40. Full UV-vis spectra (200 – 900 nm) of BSA (1 mg/mL) in 10 mM Tris-HCl buffer measured after 60 min thermal treatment (70 °C) in absence and in presence of $Au_{25}(SG)_{18}$ (30, 50, 80 and 120 µg/mL).

Further calculation of percent aggregation from data shown in Figure 38 was also made as in previous aggregation experiments with other proteins (Figure 39b). Results showed that aggregation of BSA in presence of 30 and 50 µg/mL of $Au_{25}(SG)_{18}$ nanoclusters were reduced to 70.1 and 45.8 % respectively, but in presence of 80 µg/mL, aggregation was significantly reduced to 10.6 %. These values reaffirm the chaperone-like activity of SG NCs with other proteins like BSA.

Full UV-vis spectra of BSA in absence and presence of $Au_{25}(SG)_{18}$ were also measured after thermal aggregation at 70 °C (Figure 40). Peaks at around 220 and 280 nm corresponding to the BSA were clearly distinguished. Absorption bands at 670 and 450 nm corresponding to $Au_{25}(SG)_{18}$ nanoclusters were also distinguished and became more prominent when concentration of NCs increased. The 220 nm peak corresponding to the peptide bond in the BSA moved in intensity, but it did not shift along wavelength. Peak around 280 nm corresponding to aromatic amino acids in BSA was red shifted (~20 nm) due to absorbance contribution of NCs and/or BSA-NCs interaction.

4. Discussions

Synthesis of $Au_{25}(SG)_{18}$ and $Au_{25}(Capt)_{18}$ nanoclusters were successfully achieved and confirmed with UV-vis spectrum. Synthesis of $Au_{68}(3MBA)_{32}$ nanoclusters were confirmed by the additional FTIR analysis which showed evidence of possible $Au_{68}(3MBA)_{32}$ formation.

Thermal aggregation of CS, aldolase and BSA were monitored by turbidity (OD at 360 nm). In all cases aggregation started from the beginning of the thermal treatment. In presence of Au NCs, aggregation of proteins was reduced, and this reduction was enhanced when higher concentration of nanoclusters was used.

Aggregation of CS in presence of $Au_{25}(SG)_{18}$ showed better efficiency to reduce aggregation than $Au_{25}(Capt)_{18}$. Maximum reduction was obtained to 19.4 % for GS NCs compared to 36.1 % for Capt NCs at 120 µg/mL. $Au_{68}(3MBA)_{32}$ nanoclusters showed enhanced efficiency than compared to $Au_{25}(SG)_{18}$ and $Au_{25}(Capt)_{18}$ in reducing aggregation of CS, in which aggregation was reduced to 12.5 % with lower concentration of nanoclusters (12.5 µg/mL). Aggregation of aldolase in presence of $Au_{25}(Capt)_{18}$ was more efficient to reduce aggregation than $Au_{25}(SG)_{18}$ compared at same concentration (difference of more than 21 %). Furthermore, aggregation was highly reduced to 3.1 % when $Au_{68}(3MBA)_{32}$ nanoclusters were used at lower concentration (33.4 µg/mL) than

$Au_{25}(SG)_{18}$ and $Au_{25}(Capt)_{18}$. Aggregation of BSA in presence of $Au_{25}(SG)_{18}$ was also reduced and maximum reduction to 10.6 % was obtaining when 80 µg/mL of $Au_{25}(SG)_{18}$ were used.

Effectiveness of $Au_{25}(SG)_{18}$ and $Au_{25}(Capt)_{18}$ nanoclusters to reduce aggregation depend of the protein to be studied. This could be due to the different mechanism of aggregation pathways each protein goes through. $Au_{68}(3MBA)_{32}$ nanoclusters had better efficiency to reduce aggregation than $Au_{25}(SG)_{18}$ and $Au_{25}(Capt)_{18}$ in all proteins studied in the present work. This could be due to the exceptional bioconjugation property of $Au_{68}(3MBA)_{32}$ as was reported in the literature.[9]

$Au_{25}(SG)_{18}$ nanoclusters, when added several minutes after the initiation of aggregation of CS, still manages to inhibit efficiently the further progression of aggregation, suggesting a stable interaction and formation of protein-NCs conjugate. This could give us the indication of NCs holdase activity. Full UV-vis spectra of proteins in presence of nanoclusters after thermal treatment also gives us the indication of protein-NCs interaction. The band shifts in UV region can also be from the contribution of UV absorption of nanoclusters. This protein-NCs interaction can be confirmed further by CD spectroscopy which we could not perform in the present study due to lack of time.

DLS analysis of protein aggregation (CS and aldolase) in presence of $Au_{25}(SG)_{18}$ nanoclusters confirm the effect of NCs in protein aggregation. Size of aggregated particles was reduced when aggregation of protein was performed in presence of NCs. DLS analysis of CS aggregation in presence of NCs showed that size of aggregates did not change considerably after increasing concentration of NCs, suggesting a fast saturation of aggregates with NCs. In contrast, DLS analysis of aggregation of aldolase in presence of NCs showed reduced size of aggregates when higher concentration of NCs was used, which would be due to slow saturation of aggregates with NCs.

In the present study, we successfully observed the chaperone-like activity of $Au_{25}(SG)_{18}$, $Au_{25}(Capt)_{18}$ and $Au_{68}(3MBA)_{32}$ nanoclusters. Interaction of protein with nanoclusters could be facilitated because of hydrophobic residues in intermediate unfolded proteins[50, 70] and reactivity of water-soluble nanoclusters towards polypeptides.[9, 12, 25] Presumably, nanoclusters bind initially with partially or completely unfolded proteins. This protein-nanocluster conjugate forms seeds in the nucleation stage and further adhesion of other protein-nanocluster complexes increases the size of aggregates until its saturation, which

results in aggregates with smaller size and reduced aggregation profile in turbidity measurements (Figure 41). When NCs are added several minutes after starting the aggregation of protein, they seem to present similar effect like holding chaperones, sequestering unfolded proteins and inhibiting further aggregation.

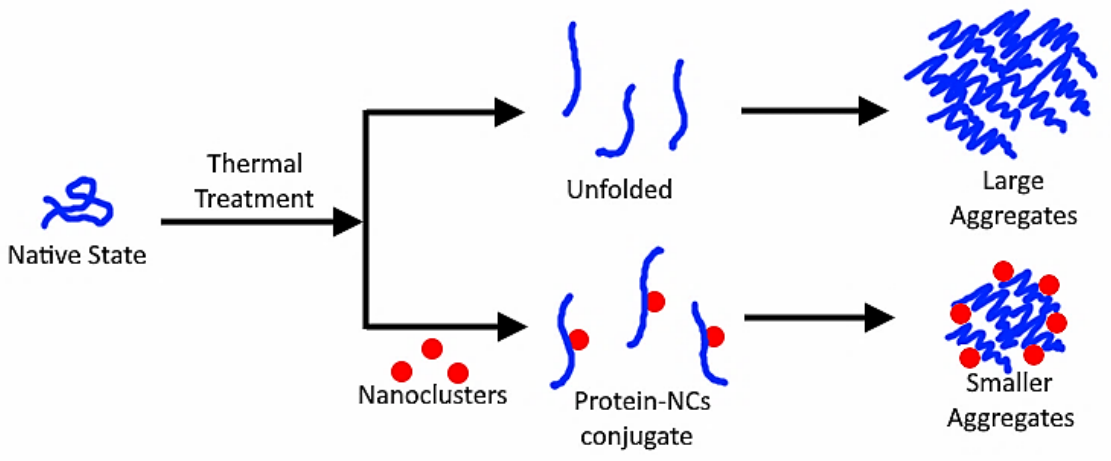

Figure 41. Schematic model for aggregation of proteins in absence and in presence of gold nanoclusters.

5. Conclusions

Chaperone-like activity of water-soluble gold nanoclusters was confirmed using CS, aldolase and BSA as protein model, and $Au_{25}(SG)_{18}$, $Au_{25}(Capt)_{18}$ and $Au_{68}(3MBA)_{32}$, as water soluble nanoclusters. $Au_{68}(3MBA)_{32}$ nanoclusters showed better efficiency to inhibit aggregation of proteins than $Au_{25}(SG)_{18}$ and $Au_{25}(Capt)_{18}$. Aggregation of proteins was reduced when Au NCs concentration was increased. This concentration-dependence effect of Au NCs was observed with all three types of NCs studied in the present work.

Reduction of protein aggregation in presence of Au NCs can be attributed to the formation of initial protein-NCs conjugate in the nucleation state, further interaction with other protein-NCs complexes cause increasing of aggregates size until its saturation and consequently reducing the hydrophobic exposure areas of proteins. Protective effect of NCs against aggregation of protein even after the initiation of aggregation after several minute proves that the NCs possess holdase activity.

This remarkable protective nature of nanocluster against protein aggregation has huge biological implication in several protein aggregations related disease which needs to be further studied in different model disease.

References

1. Wang, J.; Lin, X.; Shu, T.; Su, L.; Liang, F.; Zhang, X., Self-Assembly of Metal Nanoclusters for Aggregation-Induced Emission. *Int J Mol Sci* **2019,** *20* (8), 1891.
2. Kumar, S.; Jin, R., Water-soluble $Au_{25}(Capt)_{18}$ nanoclusters: synthesis, thermal stability, and optical properties. *Nanoscale* **2012,** *4* (14), 4222-4227.
3. Gautier, C.; Bürgi, T., Chiral Gold Nanoparticles. *ChemPhysChem* **2009,** *10* (3), 483-492.
4. Katla, S. K.; Zhang, J.; Castro, E.; Bernal, R. A.; Li, X., Atomically Precise Au25(SG)18 Nanoclusters: Rapid Single-Step Synthesis and Application in Photothermal Therapy. *ACS Applied Materials & Interfaces* **2018,** *10* (1), 75-82.
5. Brust, M.; Walker, M.; Bethell, D.; Schiffrin, D. J.; Whyman, R., Synthesis of thiol-derivatised gold nanoparticles in a two-phase Liquid–Liquid system. *Journal of the Chemical Society, Chemical Communications* **1994,** (7), 801-802.
6. Varnholt, B. Spectroscopic investigation of ligand-gold interactions in monolayer protected gold clusters. 2016.
7. Sels, A. Atomically precise metal cluster building blocks. Thèse de doctorat, Université de Genève, Genève, 2019.
8. Kang, X.; Chong, H.; Zhu, M., $Au_{25}(SR)_{18}$: the captain of the great nanocluster ship. *Nanoscale* **2018,** *10* (23), 10758-10834.
9. Azubel, M.; Kornberg, R. D., Synthesis of Water-Soluble, Thiolate-Protected Gold Nanoparticles Uniform in Size. *Nano Letters* **2016,** *16* (5), 3348-3351.
10. Chang, T.-K.; Cheng, T.-M.; Chu, H.-L.; Tan, S.-H.; Kuo, J.-C.; Hsu, P.-H.; Su, C.-Y.; Chen, H.-M.; Lee, C.-M.; Kuo, T.-R., Metabolic Mechanism Investigation of Antibacterial Active Cysteine-Conjugated Gold Nanoclusters in Escherichia coli. *ACS Sustainable Chemistry & Engineering* **2019,** *7* (18), 15479-15486.
11. Chen, Y.; Li, W.; Wang, Y.; Yang, X.; Chen, J.; Jiang, Y.; Yu, C.; Lin, Q., Cysteine-directed fluorescent gold nanoclusters for the sensing of pyrophosphate and alkaline phosphatase. *Journal of Materials Chemistry C* **2014,** *2* (20), 4080-4085.
12. Levi-Kalisman, Y.; Jadzinsky, P. D.; Kalisman, N.; Tsunoyama, H.; Tsukuda, T.; Bushnell, D. A.; Kornberg, R. D., Synthesis and Characterization of Au102(p-MBA)44 Nanoparticles. *Journal of the American Chemical Society* **2011,** *133* (9), 2976-2982.
13. Ackerson, C. J.; Jadzinsky, P. D.; Kornberg, R. D., Thiolate Ligands for Synthesis of Water-Soluble Gold Clusters. *Journal of the American Chemical Society* **2005,** *127* (18), 6550-6551.
14. Cheng, T.-M.; Chu, H.-L.; Lee, Y.-C.; Wang, D.-Y.; Chang, C.-C.; Chung, K.-L.; Yen, H.-C.; Hsiao, C.-W.; Pan, X.-Y.; Kuo, T.-R.; Chen, C.-C., Quantitative Analysis of Glucose Metabolic Cleavage in Glucose Transporters Overexpressed Cancer Cells by Target-Specific Fluorescent Gold Nanoclusters. *Analytical Chemistry* **2018,** *90* (6), 3974-3980.
15. Lakkakula, J. R.; Divakaran, D.; Thakur, M.; Kumawat, M. K.; Srivastava, R., Cyclodextrin-stabilized Gold nanoclusters for bioimaging and selective label-free intracellular sensing of Co^{2+} ions. *Sensors and Actuators B: Chemical V 262* **2018**, 270-281.
16. Xie, Y.; Xianyu, Y.; Wang, N.; Yan, Z.; Liu, Y.; Zhu, K.; Hatzakis, N. S.; Jiang, X., Functionalized Gold Nanoclusters Identify Highly Reactive Oxygen Species in Living Organisms. *Advanced Functional Materials* **2018,** *28* (14), 1702026.
17. Zang, J.; Li, C.; Zhou, K.; Dong, H.; Chen, B.; Wang, F.; Zhao, G., Nanomolar Hg^{2+} Detection Using β-Lactoglobulin-Stabilized Fluorescent Gold Nanoclusters in Beverage and Biological Media. *Analytical Chemistry* **2016,** *88* (20), 10275-10283.
18. Hu, D.; Sheng, Z.; Gong, P.; Zhang, P.; Cai, L., Highly selective fluorescent sensors for Hg^{2+} based on bovine serum albumin-capped gold nanoclusters. *Analyst* **2010,** *135* (6), 1411-1416.
19. Tseng, Y.-T.; Chang, H.-T.; Chen, C.-T.; Chen, C.-H.; Huang, C.-C., Preparation of highly luminescent mannose–gold nanodots for detection and inhibition of growth of Escherichia coli. *Biosensors and Bioelectronics* **2011,** *27* (1), 95-100.
20. Zheng, K.; Setyawati, M. I.; Leong, D. T.; Xie, J., Antimicrobial Gold Nanoclusters. *ACS Nano* **2017,** *11* (7), 6904-6910.

21. Xie, Y.; Liu, Y.; Yang, J.; Liu, Y.; Hu, F.; Zhu, K.; Jiang, X., Gold Nanoclusters for Targeting Methicillin-Resistant Staphylococcus aureus In Vivo. *Angewandte Chemie International Edition* **2018,** *57* (15), 3958-3962.
22. Ding, W.; Liu, Y.; Li, Y.; Shi, Q.; Li, H.; Xia, H.; Wang, D.; Tao, X., Water-soluble gold nanoclusters with pH-dependent fluorescence and high colloidal stability over a wide pH range via co-reduction of glutathione and citrate. *RSC Advances* **2014,** *4* (43), 22651-22659.
23. Wu, Z.; Jin, R., On the Ligand's Role in the Fluorescence of Gold Nanoclusters. *Nano Letters* **2010,** *10* (7), 2568-2573.
24. He, L.; Li, L.; Wang, T.; Gao, H.; Li, G.; Wu, X.; Su, Z.; Wang, C., Fabrication of Au/ZnO nanoparticles derived from ZIF-8 with visible light photocatalytic hydrogen production and degradation dye activities. *Dalton Transactions* **2014,** *43* (45), 16981-16985.
25. Huang, Z.; Wang, M.; Guo, Z.; Wang, H.; Dong, H.; Yang, W., Aggregation-Enhanced Emission of Gold Nanoclusters Induced by Serum Albumin and Its Application to Protein Detection and Fabrication of Molecular Logic Gates. *ACS Omega* **2018,** *3* (10), 12763-12769.
26. Roy Bhattacharya, S.; Bürgi, T., Amplified vibrational circular dichroism as a manifestation of the interaction between a water soluble gold nanocluster and cobalt salt. *Nanoscale* **2019,** *11* (48), 23226-23233.
27. Waszkielewicz, M.; Olesiak-Banska, J.; Comby-Zerbino, C.; Bertorelle, F.; Dagany, X.; Bansal, A. K.; Sajjad, M. T.; Samuel, I. D. W.; Sanader, Z.; Rozycka, M.; Wojtas, M.; Matczyszyn, K.; Bonacic-Koutecky, V.; Antoine, R.; Ozyhar, A.; Samoc, M., pH-Induced transformation of ligated Au25 to brighter Au23 nanoclusters. *Nanoscale* **2018,** *10* (24), 11335-11341.
28. McLean, A.; Wang, R.; Huo, Y.; Cooke, A.; Hopkins, T.; Potter, N.; Li, Q.; Isaac, J.; Haidar, J.; Jin, R.; Kopelman, R., Synthesis and Optical Properties of Two-Photon-Absorbing Au_{25}(Captopril)$_{18}$-Embedded Polyacrylamide Nanoparticles for Cancer Therapy. *ACS Applied Nano Materials* **2020,** *3* (2), 1420-1430.
29. Kawasaki, H.; Kumar, S.; Li, G.; Zeng, C.; Kauffman, D. R.; Yoshimoto, J.; Iwasaki, Y.; Jin, R., Generation of Singlet Oxygen by Photoexcited $Au_{25}(SR)_{18}$ Clusters. *Chemistry of Materials* **2014,** *26* (9), 2777-2788.
30. Azubel, M.; Koivisto, J.; Malola, S.; Bushnell, D.; Hura, G. L.; Koh, A. L.; Tsunoyama, H.; Tsukuda, T.; Pettersson, M.; Häkkinen, H.; Kornberg, R. D., Electron microscopy of gold nanoparticles at atomic resolution. *Science* **2014,** *345* (6199), 909-912.
31. Xie, J.; Zheng, Y.; Ying, J. Y., Protein-Directed Synthesis of Highly Fluorescent Gold Nanoclusters. *Journal of the American Chemical Society* **2009,** *131* (3), 888-889.
32. Wei, H.; Wang, Z.; Yang, L.; Tian, S.; Hou, C.; Lu, Y., Lysozyme-stabilized gold fluorescent cluster: Synthesis and application as Hg^{2+} sensor. *Analyst* **2010,** *135* (6), 1406-1410.
33. Guével, X. L.; Daum, N.; Schneider, M., Synthesis and characterization of human transferrin-stabilized gold nanoclusters. *Nanotechnology* **2011,** *22* (27), 275103.
34. Xavier, P. L.; Chaudhari, K.; Verma, P. K.; Pal, S. K.; Pradeep, T., Luminescent quantum clusters of gold in transferrin family protein, lactoferrin exhibiting FRET. *Nanoscale* **2010,** *2* (12), 2769-2776.
35. Kawasaki, H.; Yoshimura, K.; Hamaguchi, K.; Arakawa, R., Trypsin-Stabilized Fluorescent Gold Nanocluster for Sensitive and Selective Hg^{2+} Detection. *Analytical Sciences* **2011,** *27* (6), 591-591.
36. Kawasaki, H.; Hamaguchi, K.; Osaka, I.; Arakawa, R., ph-Dependent Synthesis of Pepsin-Mediated Gold Nanoclusters with Blue Green and Red Fluorescent Emission. *Advanced Functional Materials* **2011,** *21* (18), 3508-3515.
37. Liu, C.-L.; Wu, H.-T.; Hsiao, Y.-H.; Lai, C.-W.; Shih, C.-W.; Peng, Y.-K.; Tang, K.-C.; Chang, H.-W.; Chien, Y.-C.; Hsiao, J.-K.; Cheng, J.-T.; Chou, P.-T., Insulin-Directed Synthesis of Fluorescent Gold Nanoclusters: Preservation of Insulin Bioactivity and Versatility in Cell Imaging. *Angewandte Chemie International Edition* **2011,** *50* (31), 7056-7060.

38. Wen, F.; Dong, Y.; Feng, L.; Wang, S.; Zhang, S.; Zhang, X., Horseradish Peroxidase Functionalized Fluorescent Gold Nanoclusters for Hydrogen Peroxide Sensing. *Analytical Chemistry* **2011,** *83* (4), 1193-1196.
39. Yin, M.-M.; Chen, W.-Q.; Lu, Y.-Q.; Han, J.-Y.; Liu, Y.; Jiang, F.-L., A model beyond protein corona: thermodynamics and binding stoichiometries of the interactions between ultrasmall gold nanoclusters and proteins. *Nanoscale* **2020,** *12* (7), 4573-4585.
40. Hartl, F. U., Protein Misfolding Diseases. *Annual Review of Biochemistry* **2017,** *86* (1), 21-26.
41. Blanco, A.; Blanco, G., Chapter 3 - Proteins. In *Medical Biochemistry*, Blanco, A.; Blanco, G., Eds. Academic Press: 2017; pp 21-71.
42. Gromiha, M. M., Chapter 1 - Proteins. In *Protein Bioinformatics*, Gromiha, M. M., Ed. Academic Press: Singapore, 2010; pp 1-27.
43. Johns, P., Chapter 8 - Cellular mechanisms of neurological disease. In *Clinical Neuroscience*, Johns, P., Ed. Churchill Livingstone: 2014; pp 91-103.
44. Wiegand, G.; Remington, S. J., CITRATE SYNTHASE: Structure, Control, and Mechanism. *Annual Review of Biophysics and Biophysical Chemistry* **1986,** *15* (1), 97-117.
45. Buchner, J.; Grallert, H.; Jakob, U., [27] Analysis of chaperone function using citrate synthase as nonnative substrate protein. In *Methods in Enzymology*, Academic Press: 1998; Vol. 290, pp 323-338.
46. Arakaki, T. L.; Pezza, J. A.; Cronin, M. A.; Hopkins, C. E.; Zimmer, D. B.; Tolan, D. R.; Allen, K. N., Structure of human brain fructose 1,6-(bis)phosphate aldolase: linking isozyme structure with function. *Protein Sci* **2004,** *13* (12), 3077-3084.
47. Berridge, B. R.; Van Vleet, J. F.; Herman, E., Chapter 46 - Cardiac, Vascular, and Skeletal Muscle Systems. In *Haschek and Rousseaux's Handbook of Toxicologic Pathology (Third Edition)*, Haschek, W. M.; Rousseaux, C. G.; Wallig, M. A., Eds. Academic Press: Boston, 2013; pp 1567-1665.
48. Dobryszycki, P.; Rymarczuk, M.; Gapiński, J.; Kochman, M., Effect of acrylamide on aldolase structure. II. Characterization of aldolase unfolding intermediates. *Biochimica et Biophysica Acta (BBA) - Protein Structure and Molecular Enzymology* **1999,** *1431* (2), 351-362.
49. Assadpour, E.; Jafari, S. M., 1 - An overview of biopolymer nanostructures for encapsulation of food ingredients. In *Biopolymer Nanostructures for Food Encapsulation Purposes*, Jafari, S. M., Ed. Academic Press: 2019; pp 1-35.
50. Borzova, V. A.; Markossian, K. A.; Chebotareva, N. A.; Kleymenov, S. Y.; Poliansky, N. B.; Muranov, K. O.; Stein-Margolina, V. A.; Shubin, V. V.; Markov, D. I.; Kurganov, B. I., Kinetics of Thermal Denaturation and Aggregation of Bovine Serum Albumin. *PLoS One* **2016,** *11* (4), e0153495.
51. Image from RCSB PDB (www.rcsb.org) of PDB ID 5CSC (Liao, D. I.; Karpusas, M.; Remington, S. J., Crystal structure of an open conformation of citrate synthase from chicken heart at 2.8-A resolution. *Biochemistry* **1991,** *30* (24), 6031-6).
52. Image from RCSB PDB (www.rcsb.org) of PDB ID 1ADO (Blom, N.; Sygusch, J., Product binding and role of the C-terminal region in class I D-fructose 1,6-bisphosphate aldolase. *Nat Struct Biol* **1997,** *4* (1), 36-9).
53. Image from RCSB PDB (www.rcsb.org) of PDB ID 1J4E (Majorek, K. A.; Porebski, P. J.; Dayal, A.; Zimmerman, M. D.; Jablonska, K.; Stewart, A. J.; Chruszcz, M.; Minor, W., Structural and immunologic characterization of bovine, horse, and rabbit serum albumins. *Mol Immunol* **2012,** *52* (3-4), 174-82).
54. Englander, S. W.; Mayne, L., The nature of protein folding pathways. *Proceedings of the National Academy of Sciences* **2014,** *111* (45), 15873.
55. Dobson, C. M., Protein folding and misfolding. *Nature* **2003,** *426* (6968), 884-890.
56. Ferina, J.; Daggett, V., Visualizing Protein Folding and Unfolding. *Journal of Molecular Biology* **2019,** *431* (8), 1540-1564.
57. GhÉLis, C.; Yon, J., Introduction: Cellular Environment and Significance of Folding Processes. In *Protein Folding*, GhÉLis, C.; Yon, J., Eds. Academic Press: 1982; p 1.
58. Hartl, F. U.; Bracher, A.; Hayer-Hartl, M., Molecular chaperones in protein folding and proteostasis. *Nature* **2011,** *475* (7356), 324-332.

59. Roberts, C. J., Therapeutic protein aggregation: mechanisms, design, and control. *Trends Biotechnol* **2014,** *32* (7), 372-380.
60. Berrill, A.; Biddlecombe, J.; Bracewell, D., Chapter 13 - Product Quality During Manufacture and Supply. In *Peptide and Protein Delivery*, Van Der Walle, C., Ed. Academic Press: Boston, 2011; pp 313-339.
61. Tyedmers, J.; Mogk, A.; Bukau, B., Cellular strategies for controlling protein aggregation. *Nature Reviews Molecular Cell Biology* **2010,** *11* (11), 777-788.
62. Hristozova, N.; Tompa, P.; Kovacs, D., A Novel Method for Assessing the Chaperone Activity of Proteins. *PLoS One* **2016,** *11* (8), e0161970-e0161970.
63. Ben-Zvi, A. P.; Goloubinoff, P., Proteinaceous Infectious Behavior in Non-pathogenic Proteins Is Controlled by Molecular Chaperones. *Journal of Biological Chemistry* **2002,** *277* (51), 49422-49427.
64. Baneyx, F. Molecular Chaperones. https://faculty.washington.edu/baneyx/Chaperones/Chaperones.html (accessed 13 April).
65. Priya, S.; Sharma, S. K.; Goloubinoff, P., Molecular chaperones as enzymes that catalytically unfold misfolded polypeptides. *FEBS Letters* **2013,** *587* (13), 1981-1987.
66. Chevrier, D.; Chatt, A.; Zhang, P., Properties and applications of protein-stabilized fluorescent gold nanoclusters: short review. *Journal of Nanophotonics* **2012,** *6* (1), 064504.
67. Li, C.; Chen, H.; Chen, B.; Zhao, G., Highly fluorescent gold nanoclusters stabilized by food proteins: From preparation to application in detection of food contaminants and bioactive nutrients. *Critical Reviews in Food Science and Nutrition* **2018,** *58* (5), 689-699.
68. Naik, R. R.; Jones, S. E.; Murray, C. J.; McAuliffe, J. C.; Vaia, R. A.; Stone, M. O., Peptide Templates for Nanoparticle Synthesis Derived from Polymerase Chain Reaction-Driven Phage Display. *Advanced Functional Materials* **2004,** *14* (1), 25-30.
69. Saibil, H., Chaperone machines for protein folding, unfolding and disaggregation. *Nature Reviews Molecular Cell Biology* **2013,** *14* (10), 630-642.
70. Das, A.; Chakrabarti, A.; Das, P. K., Suppression of protein aggregation by gold nanoparticles: a new way to store and transport proteins. *RSC Advances* **2015,** *5* (48), 38558-38570.
71. Singha, S.; Bhattacharya, J.; Datta, H.; Dasgupta, A. K., Anti-glycation activity of gold nanoparticles. *Nanomedicine: Nanotechnology, Biology and Medicine* **2009,** *5* (1), 21-29.
72. Ahmed, F.; Husain, Q., Suppression in advanced glycation adducts of human serum albumin by bio-enzymatically synthesized gold and silver nanoformulations: A potential tool to counteract hyperglycemic condition. *Biochimie* **2019,** *162*, 66-76.
73. Chakraborty, A.; Biswas, A., Structure, stability and chaperone function of Mycobacterium leprae Heat Shock Protein 18 are differentially affected upon interaction with gold and silver nanoparticles. *International Journal of Biological Macromolecules* **2020,** *152*, 250-260.
74. Seneviratne, C.; Narayanan, R.; Liu, W.; Dain, J. A., The in vitro inhibition effect of 2nm gold nanoparticles on non-enzymatic glycation of human serum albumin. *Biochemical and Biophysical Research Communications* **2012,** *422* (3), 447-454.
75. Gliniewicz, E. F.; Chambers, K. M.; De Leon, E. R.; Sibai, D.; Campbell, H. C.; McMenimen, K. A., Chaperone-like activity of the N-terminal region of a human small heat shock protein and chaperone-functionalized nanoparticles. *Proteins: Structure, Function, and Bioinformatics* **2019,** *87* (5), 401-415.
76. Singha, S.; Datta, H.; Dasgupta, A. K., Size Dependent Chaperone Properties of Gold Nanoparticles. *Journal of Nanoscience and Nanotechnology* **2010,** *10* (2), 826-832.
77. Myers, J. A.; Curtis, B. S.; Curtis, W. R., Improving accuracy of cell and chromophore concentration measurements using optical density. *BMC Biophysics* **2013,** *6* (1), 4.
78. Wang, K.; Kurganov, B. I., Kinetics of heat- and acidification-induced aggregation of firefly luciferase. *Biophysical Chemistry* **2003,** *106* (2), 97-109.
79. Sankhala, R. S.; Damai, R. S.; Swamy, M. J., Correlation of Membrane Binding and Hydrophobicity to the Chaperone-Like Activity of PDC-109, the Major Protein of Bovine Seminal Plasma. *PLoS One* **2011,** *6* (3), e17330.
80. Joshi, D.; Soni, R. K. In *Laser induced gold nanoparticle egg-white protein conjugation and thermal denaturation*, 2012 International Conference on Fiber Optics and Photonics (PHOTONICS), 9-12 Dec. 2012; 2012; pp 1-3.

81. Fernandez-Funez, P.; Sanchez-Garcia, J.; de Mena, L.; Zhang, Y.; Levites, Y.; Khare, S.; Golde, T. E.; Rincon-Limas, D. E., Holdase activity of secreted Hsp70 masks amyloid-β42 neurotoxicity in *Drosophila*. *Proceedings of the National Academy of Sciences* **2016,** *113* (35), E5212-E5221.
82. Ray, N.; Roy, S.; Singha, S.; Chandra, B.; Dasgupta, A. K.; Sarkar, A., Design of Heat Shock-Resistant Surfaces to Prevent Protein Aggregation: Enhanced Chaperone Activity of Immobilized α-Crystallin. *Bioconjugate Chemistry* **2014,** *25* (5), 888-895.